ANL-75-57

ANL-75-57

SUMMARY AND EVALUATION - FUEL DYNAMICS LOSS-OF-FLOW EXPERIMENTS (TESTS L2, L3, AND L4)

by

E. W. Barts, L. W. Deitrich, J. G. Eberhart,
A. K. Fischer, and C. C. Meek

BASE TECHNOLOGY

U of C-AUA-USERDA

ARGONNE NATIONAL LABORATORY, ARGONNE, ILLINOIS

Prepared for the U.S. ENERGY RESEARCH AND DEVELOPMENT ADMINISTRATION
Division of Reactor Research and Development
under Contract W-31-109-Eng-38

DISCLAIMER

Printed in the United States of America
Available from
National Technical Information Service
U. S. Department of Commerce
5285 Port Royal Road
Springfield, Virginia 22161
Price: Printed Copy $5.45; Microfiche $2.25

Distribution Category:
LMFBR Safety (UC-79p)

ANL-75-57

ARGONNE NATIONAL LABORATORY
9700 South Cass Avenue
Argonne, Illinois 60439

SUMMARY AND EVALUATION - FUEL DYNAMICS LOSS-OF-FLOW EXPERIMENTS (TESTS L2, L3, AND L4)

by

E. W. Barts, L. W. Deitrich, J. G. Eberhart,*
A. K. Fischer,* and C. C. Meek

Reactor Analysis and Safety Division

September 1975

*Chemical Engineering Division, ANL

THIS PAGE

WAS INTENTIONALLY

LEFT BLANK

TABLE OF CONTENTS

TABLE OF CONTENTS

LIST OF FIGURES

LIST OF FIGURES

LIST OF FIGURES

LIST OF TABLES

SUMMARY AND EVALUATION - FUEL DYNAMICS LOSS-OF-FLOW EXPERIMENTS (TESTS L2, L3, AND L4)

by

E. W. Barts, L. W. Deitrich, J. G. Eberhart, A. K. Fischer, and C. C. Meek

ABSTRACT

Three similar experiments conducted to support the analyses of hypothetical LMFBR unprotected-loss-of-flow accidents are summarized and evaluated in this report. The tests, designated L2, L3, and L4, provided experimental data against which accident-analysis codes could be compared, so as to guide further analysis and modeling of the initiating phases of the hypothetical accident. The tests were conducted using seven-pin bundles of mixed-oxide fuel pins in Mark-II flowing-sodium loops in the TREAT reactor.

Test L2 used fresh fuel. Tests L3 and L4 used irradiated fuel pins having, respectively, "intermediate-power" (no central void) and "high-power" (fully developed central void) microstructure. The report does not include the posttest examination results for L3 and L4, nor does the report contain the final hodoscope results. Conclusions based on the available test data are presented with particular emphasis on fuel dynamics.

I. INTRODUCTION

A. Purpose and Scope

An important effort in support of the Final Safety Analysis Report for the FTR is an analysis of a hypothetical unprotected pump-coastdown accident, a loss-of-flow to the whole core with assumed failure to scram. In support of this analysis the Fuel Dynamics Program at ANL conducted three TREAT experiments using seven-pin bundles of mixed-oxide fuel pins in Mark-II loops. These tests, designated L2, L3, and L4,[1-3] were intended to provide experimental data against which predictions of the accident analysis codes can be compared, and to guide the further analysis and modeling of the initiating phases of the hypothetical accident. This report presents a brief discussion of the design of the experiments and a summary of the test data. The data are then discussed with respect to boiling inception, voiding nature, dryout and fuel-pin failure, initial fuel motion, molten-clad dynamics, molten-fuel dynamics, and flow blockages. The tests are related to the FTR loss-of-flow accident. The results of the SAS[4] calculations are presented in the Appendix.

B. The Fuel Dynamics Loss-of-flow Test Program

Test L2, the first of the three tests, used fresh fuel pins. A previous test, L1,[5] was conducted using a single, fresh, fuel pin. In this test fuel-pin failure was not planned although the failure threshold was closely approached. Thus, test L2 was the first in which fuel-pin destruction due to loss of flow occurred. Subsequent tests L3 and L4 used EBR-II-irradiated fuel pins having, respectively, "intermediate-power" (no central void) and "high-power" (fully developed central void) microstructure. An important objective of the test series was to obtain comparative data on the behavior of fresh and irradiated fuel. These tests provide the only such data available at present.

Phenomena expected during tests L2, L3, and L4 included heating of the fuel and clad, coolant boiling and voiding of the heated zone (possibly influenced by fission-gas release), cladding melting and relocation, and fuel melting and relocation. Features common to the three tests include the general character of the power-transient and flow-coastdown shapes, the initial temperature, the power distribution, and the length of the fuel column. There is no feedback from the test to the TREAT reactor, and no attempt to simulate the power bursts resulting from reactivity changes due to voiding or material motion was made in these tests.

Other tests related to the loss-of-flow accident analysis include the R-series, OPERA tests, F-series, and EOS-series. The R-series (in-pile) and OPERA tests (out-of-pile) provide much more detailed hydraulic simulation of fuel pins in the FTR core. Full-length fuel columns (36 in.) are used in the R-series, along with graded fuel enrichment and small spacer wires on peripheral pins. These measures produce a nearly uniform temperature in all subchannels so that coolant voiding is nearly one-dimensional. However, neither mixed-oxide nor preirradiated fuel can be used in the R-series apparatus. The OPERA experiments are basically out-of-pile duplicates of the R-series tests, but with more extensive instrumentation. Both the F-series and the EOS-series tests are intended to obtain in-pile data on fuel motion under specific conditions expected during the loss-of-flow accident sequences.

C. Summary of Status

This report is based on information available as of about February 1, 1974. It does not reflect the posttest examination results for tests L3 or L4, nor does it reflect final hodoscope results for these tests. Table I summarizes the status of work on the three tests discussed in this report.

D. Summary and Conclusions

Each experiment had a heat-balance run and a loss-of-flow run. Each loss-of-flow run was similar in performance, that is, in each experiment, after a short preheat, the flow was reduced to a predetermined value while the fuel-pin power was maintained constant until the reactor was scrammed. Once flow was reduced, the pump voltage was held constant for the remainder of each test. Power was maintained as long as possible within

TABLE I. Status of Loss-of-flow Tests

Test	Neutron Radiography	Hodoscope Analysis	Posttest Examination	SAS Calculations
L2	C	C	C	C
L3	C	I	N	C
L4	C	I	N	C

C = Work Complete

I = Interim Results Available

N = Work Not Included

the TREAT operating constraints. The controlled test parameters in each experiment were similar. The sequence of events in each experiment was similar, but differences were observed between the behavior of fresh and preirradiated fuel.

Experiments L2, L3, and L4 and the test apparatus are described in Sect. II. The test results are presented in Sect. III. A more detailed description of the tests will be found in the individual reports prepared for each experiment.[1-3] Section IV provides an interpretation of the test results, with particular emphasis on fuel motion. Section V relates the tests to FTR. The SAS calculations performed are summarized in the Appendix.

The following paragraphs summarize the test results and give preliminary conclusions based upon the current available test data. Final individual reports are under preparation which include completed hodoscope-data analysis and posttest-examination results.

1. Boiling Inception

The start of coolant boiling was clearly indicated in all three experiments by fluctuations in coolant flow and local thermocouple temperature readings. Within a second after boiling inception a total cessation of flow was observed. This implies a bulk boiling across an entire test-section cross section.

2. Voiding Nature

Marked expansion and collapse of voids occurred during the fresh-fuel experiment. On the other hand, oscillations tended to be damped out in the preirradiated-fuel tests. Coolant voiding was apparently influenced by the release of gas from the fuel pins near the time of fuel-pin failure.

3. Clad Dryout and Fuel-pin Failure

Fuel-pin failure and the processes of both clad and structure dryout were clearly indicated during the experiments with preirradiated fuel. The gas release was gradual during fuel-pin failure. The fuel pins failed near the time that the cladding became molten. The entire phenomenon of coolant boiling and voiding and clad dryout in a seven-pin bundle is complex and not readily modeled by existing codes.

4. Initial Fuel Motion

Considerable prefailure bowing of the fuel pin occurred in all three tests. The prefailure fuel-pin motion adds to complexity of the entire accident sequence, for deformations can influence local coolant flow and temperature.

5. Molten-clad Dynamics

Clad and other stainless steel motion cannot be directly observed during an experiment. Some clad apparently moved upward, but the majority of the molten steel moved downward to freeze in the lower part of the test section near the end of the original fuel column. As the fuel moved downward, it remelted the steel frozen beneath it.

6. Molten-fuel Dynamics

The fresh fuel collapsed shortly after the cladding melted, probably due to a breaking apart of the now unclad pellet stack. In contrast, preirradiated fuel remained essentially in place after the cladding melted. This difference in behavior was most likely due to a combination of causes. The most important one is swelling of the preirradiated fuel. Any collapse of preirradiated fuel was most likely due to fuel melting.

Molten fuel occurred in all three experiments. Shortly after the fuel became molten, eructations or abrupt fuel motions were observed. The abrupt motion of the fuel can be attributed to the vaporization of stainless steel trapped in the molten fuel. This steel could have been some of that melted by the falling molten fuel, the lighter steel rising through the fuel.

7. Flow Blockages

Solid flow blockages were formed near the bottom of the original fuel column in all three experiments. Frozen fuel tended to be porous in nature, but frozen steel was solid.

II. TEST DESCRIPTION

A. TREAT Reactor

Experiments L2, L3, and L4 were conducted in the TREAT Facility[6] at NRTS, Idaho. TREAT is a UO_2-fueled, graphite-moderated thermal reactor incorporating a computer-controlled feedback-control system. The control system permits a wide variety of shaped power transients to be produced. The duration of possible transients is limited by the maximum allowable TREAT fuel temperature (600°C) and by the reactivity available to overcome temperature feedback. Slotted fuel elements allow observation of experiments in the center of the core. A schematic of the reactor is shown in Fig. 1.

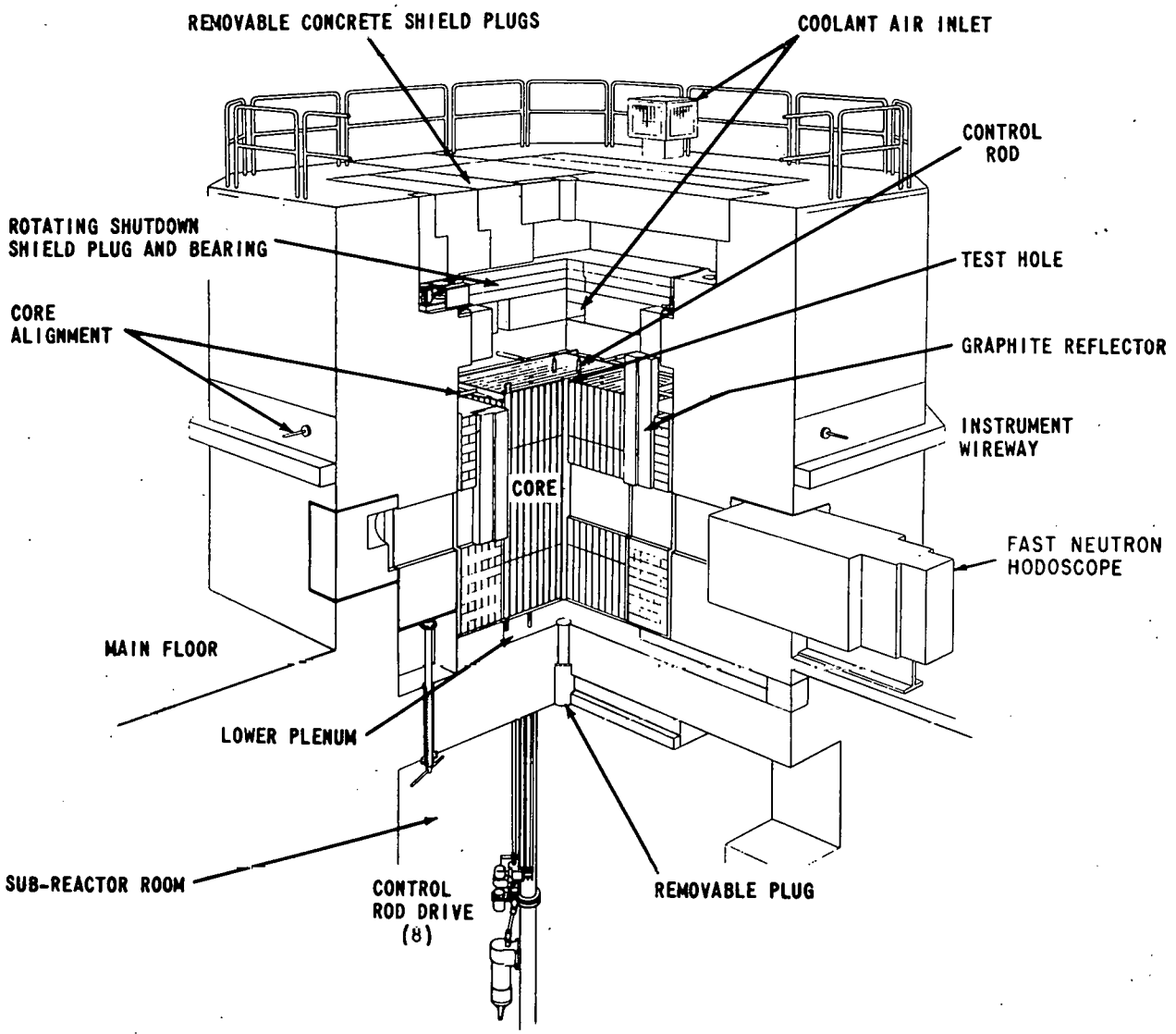

Fig. 1. Schematic of the TREAT Reactor. ANL Neg. No. 900-2776.

B. Mark-II Loop

The test vehicle for the L-series experiment is the Mark-II integral loop.[7] This package loop replaces two TREAT fuel elements at the center of the core. A diagram of the loop is shown in Fig. 2. Sodium is circulated

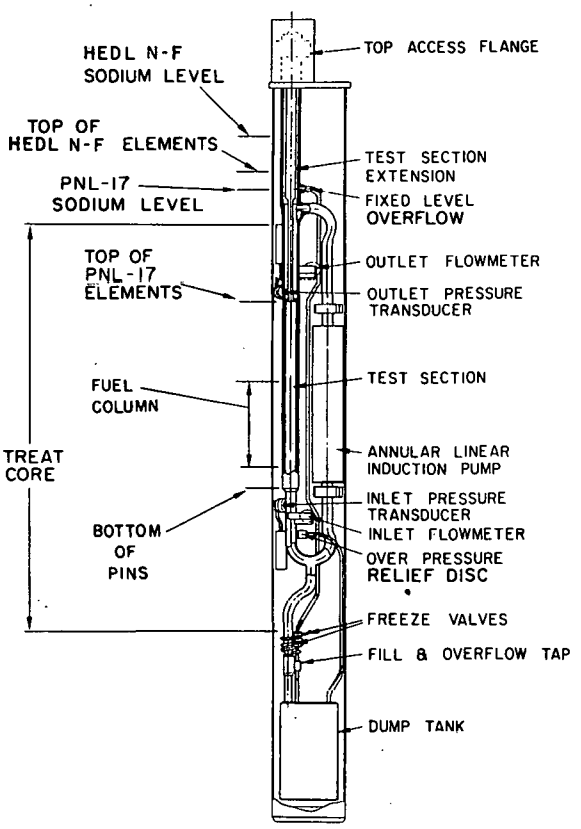

Fig. 2.
Schematic of the Mark-II Loop.
ANL Neg. No. 900-2777 Rev. 1.

downward through the annular linear induction pump and upward over the fuel pins located in the test section. The loop piping has an inside diameter of 0.75 in. The flow path in the pump is a 1.05- by 0.75 in. annulus. The hydraulic dimensions of the balance of the flow path is determined from the test-section geometry.

Certain test instrumentation is provided with the loop body. Pressure transducers and flowmeters are located above and below the fuel column. The flowmeters are an electromagnetic type, excited by an external, constant-current, dc power supply. The pressure transducers are 2500-psi-rated-range, unbonded strain-gauge units excited at 5 kHz, 5 V rms, by an external oscillator-demodulator unit. Each pressure transducer is mounted on a NaK-filled standoff tube which allows enough room for the mounting and which separates the transducer from the loop sufficiently to keep the transducer temperature within allowable limits. The NaK is separated from the loop sodium by a bellows. Thermocouple instrumentation for each test is built into the test section.

C. Test Section

An "adiabatic," fluted-tube, fuel holder was used for tests L2, L3, and L4. A cross-sectional view of the test section, taken through the fuel column region, is shown in Fig. 3. The seven-pin bundle is contained

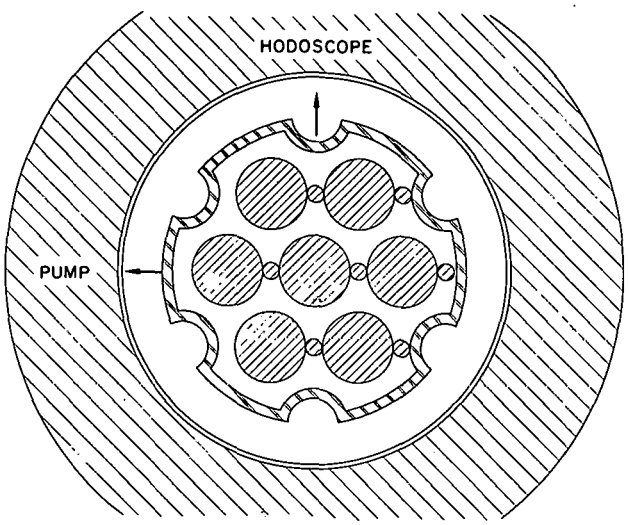

Fig. 3.
Test-section Cross Section.
ANL Neg. No. 900-2865 Rev. 1.

within a flow tube in which flutes are pressed at the approximate locations of the next adjacent fuel pins. A gas-filled space surrounds the fluted tube to minimize radial heat transfer. In test L2, this space was occupied by the circuitry required for an experimental void detector. In tests L3 and L4, thermocouples were attached to the outside of the fluted tube at various axial locations. Figure 4 is an axial schematic of the test section. The dysprosium flux-shaping collars were located to eliminate end peaking of the pin power and thus produce an acceptable axial power distribution. Full thermal-neutron filtering was not used in the experiments.

Seven thermocouples were provided in the L2 test section. Two of them, numbers 1 and 7, were located about 1/4 in. below the entrance of the pin bundle in the sodium flow stream. One thermocouple, number 4, was located within the pin bundle with its junction approximately at the level of the top of the fuel column. The remaining four thermocouples were located at the outlet from the pin bundle. All thermocouples were 0.040-in.-dia, stainless steel-sheathed, chromel-alumel wire. The nominal thermocouple time constant for response to temperature change was 30 msec.

Fourteen thermocouples were provided in the L3 and L4 test sections. Thermocouples number 1 and number 2 were located in the inlet sodium in a location similar to those at the pin-bundle entrance in L2. Thermocouples numbered 3, 4, 5, and 6 were situated in the outlet sodium; their junctions were approximately in a plane 1/8 to 1/4 in. above the top end of the fuel pins. These six thermocouples measured sodium temperatures directly. The junctions of the eight remaining thermocouples were welded to the outside of the fluted tube at various points and thus measured structure temperature. Thermocouples 10 through 14 were adjacent to points on the fuel column. Thermocouples 7, 8, and 9 were located above the tops of the fuel column. The thermocouple locations are shown in Figs. 5 and 6.

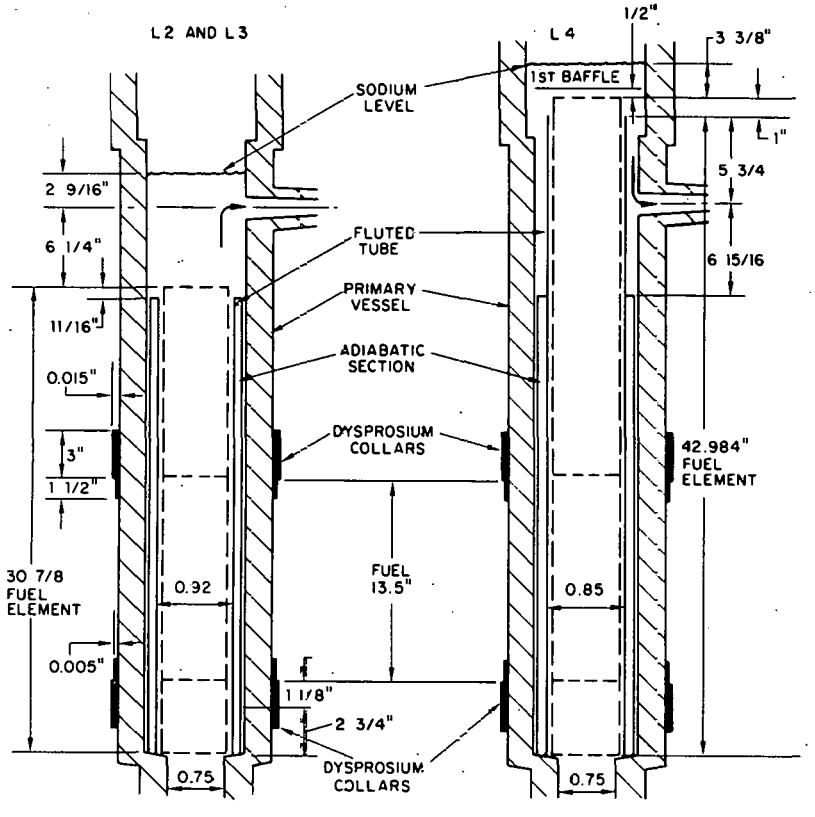

Fig. 4. Schematic of Axial Test Section.

Inlet Thermocouples in (L2), L3, and L4

TC1 (TC1) is located at the test section half-radius
TC2 (TC7) is located at the test section centerline

Outlet Thermocouples in (L2), L3, and L4

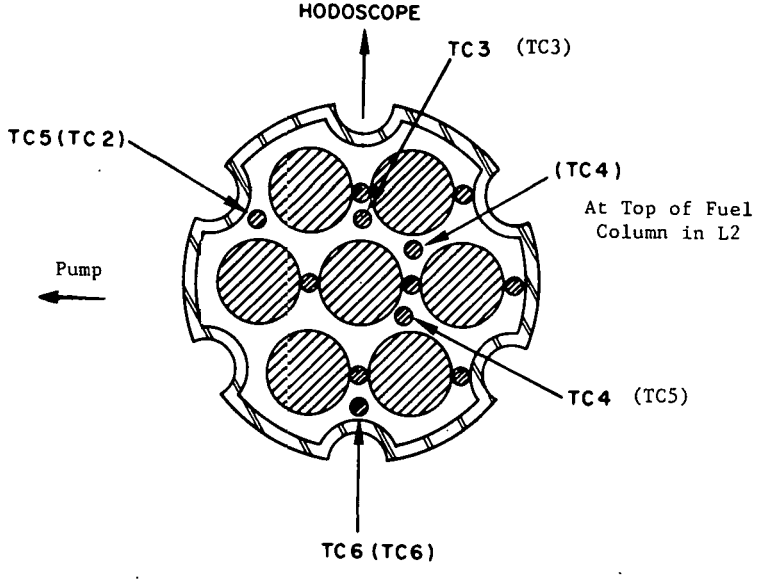

Fig. 5. Radial Location of Sodium Inlet and Outlet Thermocouples.

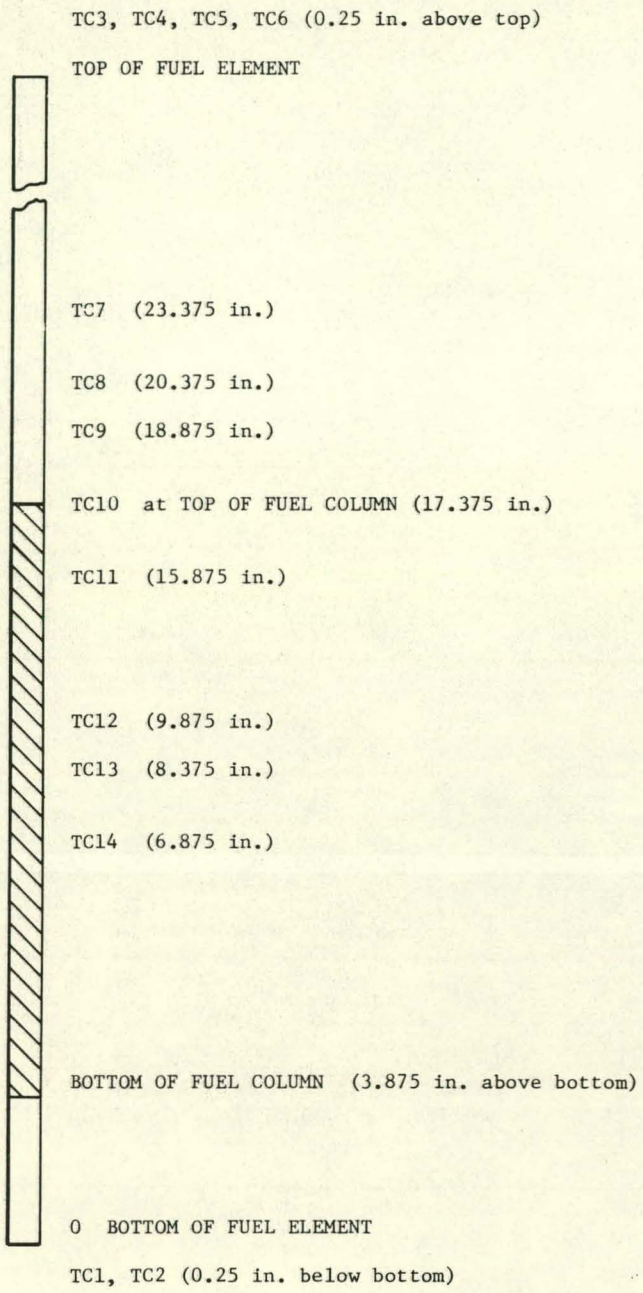

Fig. 6. Axial Location of Sodium Inlet and Outlet Thermocouples.

An instrument unique to test L2 among Fuel Dynamics tests is the void detector. This experimental instrument was included in the hope that definitive data on the growth and collapse of voids, other than that gained from flowmeters, could be obtained. However, mechanical difficulties associated with the limited space available resulted in failure to obtain useful data.

D. Fuel Pins

Figure 7 is a schematic drawing of the test fuel pins. Important fuel-element parameters are summarized in Table II. The pins in L2 were used "as fabricated." The L3 and L4 pins were irradiated in EBR-II and then modified for use in the tests.

The early part of the irradiation of the PNL-17 type pins used in test L3 was done at a maximum power of 9.2 kW/ft. During the later part, the pins were irradiated at 11.5 kW/ft. The total burnup was 3.5 a/o. As can be seen in Fig. 8, the microstructure of the fuel was characteristic of the lower power level, that is, no central void formed. However, the part of the irradiation that was done at the higher power rating promoted release of fission gas to the pin plenum so that the pin, though having a low-power microstructure, retained less gas than usual for such a structure. After irradiation, the pins were shortened to fit the test section by cutting 9-3/8 in. from the top end plug, leaving an overall pin length of 30-7/8 in.

The HEDL N-F type of fuel pins used in test L4 were irradiated to 4.3-a/o burnup at 14 kW/ft. Examination of a sibling fuel pin (see Fig. 9) showed the central void, columnar grain growth, equiaxed grain region, and unrestructured region characteristic of high-power-irradiated oxide fuel.

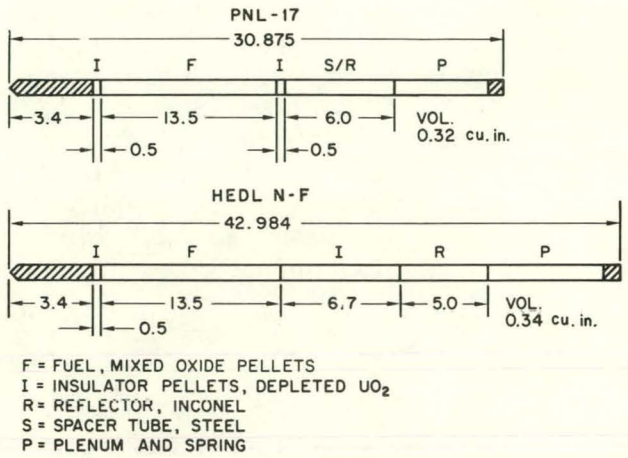

Fig. 7.
Schematic of Fuel Elements.
ANL Neg. No. 900-3249 Rev. 1.

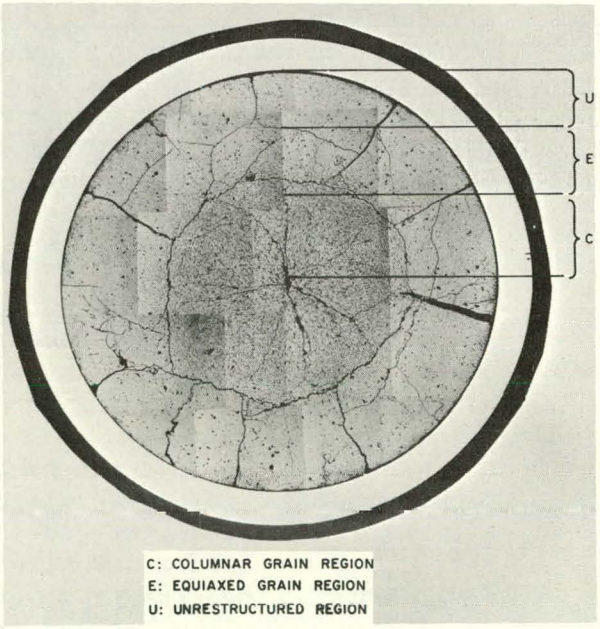

Fig. 8.
Metallographic Cross Section of Type of Fuel Pin Used in Test L3.
ANL Neg. No. 900-4006.

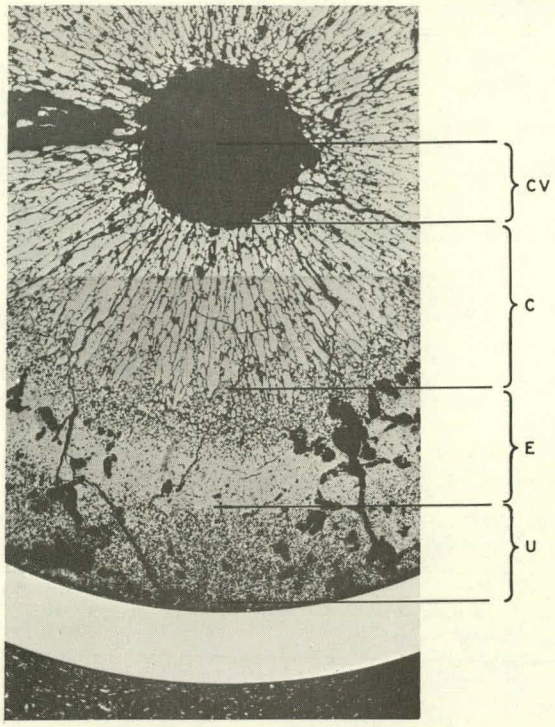

CV: CENTRAL VOID E: EQUIAXED GRAIN REGION
C : COLUMNAR GRAIN REGION U: UNRESTRUCTURED REGION

Fig. 9.
Metallographic Cross Section of Type of Fuel Pin Used in Test L4.
ANL Neg. No. 900-4005.

E. Fast-neutron Hodoscope

Direct observation of fuel motion is provided by the fast-neutron hodoscope,[8] a multichannel collimated device with high specific sensitivity to fission neutrons. Fissioning material in a test loop or capsule can be detected and the position determined even when the sample is surrounded by substantial amounts of sodium and steel.

To determine the presence of fuel, the hodoscope detects high-energy neutrons from the fission process. A 334-channel hodoscope collimator is at the edge of the reactor, aimed into an open slot through the TREAT core. There are 334 neutron detectors, each positioned behind a slot in the collimator. The collimator focuses upon a 2 x 20-in. area framing the test fuel at the center of the core. Horizontal detector separation is 150 mils and vertical detector separation is 7/8 in. Time resolution was specified at 12 msec. Most of the data were later integrated over 72-msec intervals. Signal-to-background ratio for the fuel-pin cluster considered as a unit was about 10 to 1.

Data from the hodoscope detectors are recorded on photographic film. Several computer-managed steps are required for data reduction. The most useful output format for quantative analysis are normalized count rates plotted as a function of time. In examining the data, one should remember that the hodoscope provides a two-dimensional display of a three-dimensional experiment.

TABLE II. Fuel-element Parameters

Fuel (FTR Type)	L2	L3	L4
Length, in.	13.5	13.5	13.5
Smear density, %	88	88	86
Composition,* w/o UO_2	75	75	75
w/o PuO_2	25	25	25
Enrichment,* w/o ^{235}U in U	65	65	77
w/o $^{239}Pu + ^{241}Pu$ in Pu	88	89	88
Nominal burnup, a/o	0.0	3.5	4.3
Average irradiation power, kW/ft	-	9.2-11.2	14.0
Space-wire diameter, in.	0.054	0.054	0.040
Overall pin length, in.	30.875	30.875	42.984
Insulator pellets, depleted UO_2	0.5 in. at top and bottom	0.5 in. at top and bottom	6.7 in. at top and 0.5 in. at bottom
Inconel reflector	6 in. at top	none	5 in. at top
Gas-plenum volume, cu. in.	0.15	0.32	0.34
Gas-plenum pressure (67°F), psi	15	72.5	165

*As fabricated.

F. Test Transients

In keeping with the test objective of comparing behavior of different fuel samples under loss-of-flow conditions, the three tests were run with similar power transients, initial temperatures, and flow-coastdown characteristics.

All tests used a power transient having a 2-sec-long preheat phase followed by a constant-power phase during which flow coastdown and succeeding events took place. The cluster-average linear power levels and other parameters defining the transients are given in Table III. The

TABLE III. Test Parameters

Test Designation	L2	L3	L4
Fuel-pin Power			
Preheat phase, kW/ft	18.0	16.1	17.0
Sustained phase, kW/ft	10.9	9.3	10.0
Start of sustained phase, sec	7.5	7.2	7.2
Reactor scram, sec	31.1	34.0	30.2
Loop Flow			
Initial, gpm	14.5	14.4	11.8
Reduced,* gpm	1.4	2.0	1.5
Start of decrease, sec	9.2	9.4	7.0
End of decrease, sec	17.0	13.8	12.2

*Single-phase flow at pump-control setting.

preheat phase accelerated the attainment of coolant and fuel temperatures representative of steady-state operation so that a longer time at steady power was achieved within TREAT operating limits. Note that power bursts were not simulated. The sustained power level in L2 was selected to approximate the average value in the upper third of the hottest FTR pin (with 15% overpower), whereas the levels for L3 and L4 were selected to achieve roughly the fuel temperatures at which the pins had been irradiated.

Similar flow transients were used in all three tests. A nominal initial velocity of 5 m/sec was maintained until steady power was reached in L4 and for 2 sec longer in L2 and L3. The pump power was then decreased by a servo system until a nominal 10% of the initial flow was reached. This level of pump power was maintained throughout the transient. In general, the initial flow was about 2/3 of the nominal FTR value. The flow decrease was considerably more rapid than would occur in the FTR. This produced a nonprototypic temperature distribution above the fuel at the inception of boiling. However, as will be shown in Sect. V, the nonprototypic axial temperature profile in that region was erased long before fuel motion occurred.

All three tests had a nominal initial temperature of 860°F. A rise in sodium inlet temperature of about 100°F occurred during the preheat and flow-coastdown phases of the test. This temperature rise terminated when loop flow stopped at the inception of boiling.

III. EXPERIMENT RESULTS

A. Test Scenarios

Analysis of test data has concentrated on extraction of information related to coolant voiding; clad melting and motion; and fuel melting and motion. In general, the irradiated fuel during tests L3 and L4 behaved similarly, differing markedly from that of the fuel during L2. Test power and flow histories of the experiments L2, L3, and L4 are given in Figs. 10, 11, and 12, respectively. Test data and sequences of events are summarized in the form of a scenario in Tables IV, V, and VI, respectively. Significant test events are compared in Table VII. Note the sequence of events for all experiments are similar in both order and time intervals.

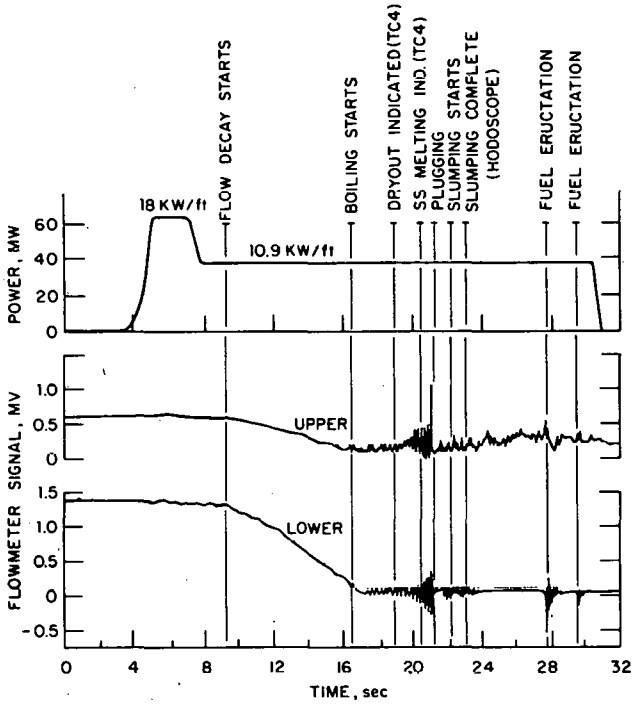

Fig. 10.
Test L2 Power and Flow Data.

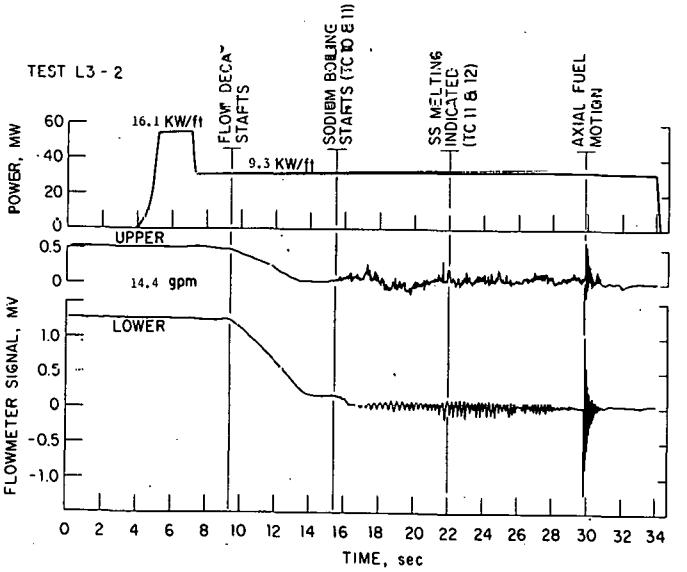

Fig. 11.
Test L3 Power and Flow Data.
ANL Neg. No. 900-2940.

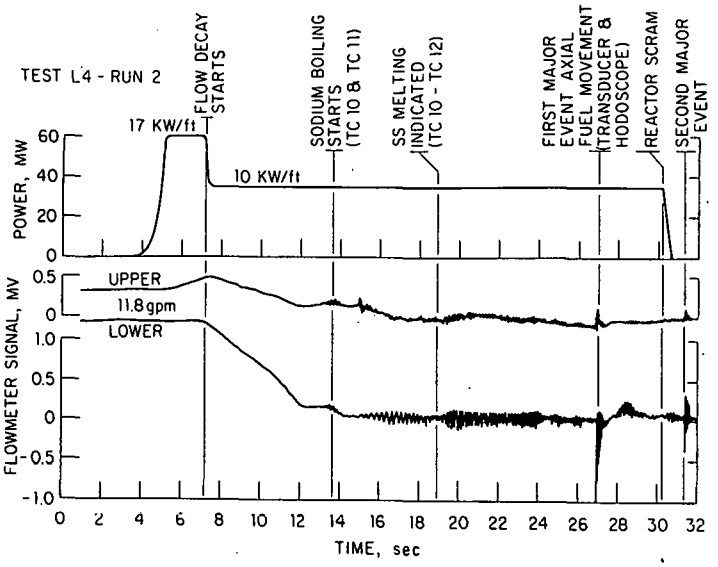

Fig. 12.
Test L4 Power and Flow Data.
ANL Neg. No. 900-2939 Rev. 2.

B. Special Scenario Events

1. Boiling Inspection

The initiation of local boiling is clearly indicated in all three experiments. In the experiments flowmeter oscillations were observed when the temperature at the top of the fuel column reached a level equal to the boiling temperature of sodium.

Less than a second after the initiation of local boiling the flow in all three experiments effectively ceased. This is an indication of bulk sodium boiling with vapor flow predominating in all channels across the entire test cross section. At this time temperature rises indicated by the thermocouples above the fuel column began to level off. The data imply that boiling started at a hot spot, possibly under a spacer wire near the top of the fuel column on the pin furthest away from the pump (the hottest pin) and progressed over the entire bundle cross section during an interval from 0.6 to 0.9 sec.

2. Voiding Nature

Some information on coolant boiling and voiding patterns can be derived from thermocouple and flowmeter data. After the initiation of boiling, prominent flow oscillations developed in L2, and smaller oscillations were observed in L3 and L4.

The L-series experiments are not designed to produce one-dimensional voiding due to sodium boiling. On the other hand, data obtained can be compared to results derived from existing analytical models. The data unfortunately have considerable uncertainty. The full-scale flowmeter reading is 5 mV or a flow of about 17.5 m/sec for the lower flowmeter. Measurements in L2 after flow reduction and start of boiling are at the 0.1-mV level (35 cm/sec) and oscillate to as high as 0.5 mV (175 cm/sec). The uncertainty of the flowmeter instrument readings is of

TABLE IV. Scenario of Events for Test L2

Time (sec	Event
0.0	Beginning of test; temperature 885°F; flow, 14.5 gpm.
5.25 to 7.25	18-kW/ft power preheat.
8.0	10.9 kW/ft steady-state power.
9.2	Flow reduction starts.
16.4	Sodium boiling begins; temperature at top of fuel column (TC4) at plateau of 1740°F; flowmeter and outlet temperature oscillations start.
17.0	Flow rate down to 1.4 gpm.
17.3	Effective flow cessation; zero net flow.
19	Dryout suggested; TC4 completes slow rise to 1800°F; outlet temperatures increase.
20.5	Stainless steel melting indicated; TC4 reaches 2550°F.
21.1 to 21.3	Flow blockage indicated; marked ejections of sodium from test-section outlet followed by cessation of flow oscillations; peak outlet temperatures observed.
21.5	TC4 fails.
22.2 to 22.5	Inlet thermocouples (TC1 and TC7) fail; fluted-tube melting indicated.
22.3	Fuel slumping observed by hodoscope.
23.7	Start of quiet period observed by hodoscope.
27.7 (27.679 to 27.706)	First eructation of fuel upward observed by hodoscope; flowmeter signals and coherent outlet thermocouple rises observed.
28.7	Slumping of ejected fuel almost complete as observed by hodoscope.
29.5	Second major eructation observed by hodoscope.
30.9	Slumping nearly complete observed by hodoscope.
31.1	Reactor scram.

TABLE V. Scenario of Events for Test L3

Time (sec)	Event
0.0	Beginning of test; temperature ≈883°F; flow, 14.4 gpm.
5.1 to 7.1	16.1-kW/ft power preheat.
7.25	9.3-kW/ft steady-state power.
9.4	Flow reduction starts.
14.6	Flow rate down to 2.0 gpm.
15.6	Sodium boiling begins; flowmeter deviations observed; fluted-tube thermocouples near top of fuel column (TC10 and TC11) show temperature leveling off at 1800°F.
15.8 to 16.2	Effective flow cessation; fluted-tube thermocouples above fuel column (TC7, TC8, and TC9) indicate temperature leveling off at 1800°F.
17.5	Dryout of cladding and pin failure suggested; fluted-tube thermocouples (TC7, 8, 9, 10, 11, and 12) begin gradual temperature rise; pressure transducers begin gradual rise.
19	End of gas release from pin and start of fluted-tube dryout suggested; end of gradual temperature and pressure rises.
22.0	Stainless steel melting indicated by the thermocouple failure; TC1, TC11, and TC12 all fail about this time; TC10 temperature rose to about 2520°F and then failed at 24.6 sec.
29.8 to 30.5	Fuel motion in axial direction observed by hodoscope; flow perturbations, inlet pressure transducer excursions, and thermocouples above fuel column (TC7, TC8, and TC9) showed temperature spike.
34.0	Reactor scram.

TABLE VI. Scenario of Events for Test L4

Time (sec)	Event
0.0	Beginning of test; temperature, ≈860°F; flow, 11.8 gpm.
5.1	Power reaches preheat level of 17 kW/ft.
7.2	Flow reduction begins.
7.4	Power reaches steady-state level of 10 kW/ft.
7.5	Fuel pins bow toward pump.
10.0	Bowing becomes increasingly noncoherent until ∿14 sec.
12.0	Flow rate down to 1.5 gpm.
13.4	Sodium boiling begins; initiation of oscillations in flowmeters; beginning of temperature plateau at 1750°F on fluted tube near top of fuel column (TC11).
14.0	Radial fuel expansion begins and continues until ∿20 sec.
14.2	Effective flow cessation.
15.3	Dryout of cladding and pin failure suggested; end of temperature plateau at 1750°F for fluted-tube thermocouples (TC7-TC12); start of pressure rise; beginning of pin motion away from pump; motion continues to 17.5 sec.
16.4	End of gas release from pin and start of fluted-tube dryout; end of gradual temperature and pressure rise.
18.9	Top portion of fuel on the side away from the pump pushed through the fluted tube up to test-section wall; motion continues to 20.0 sec; melting of fluted tube indicated; beginning of a temperature plateau at 2510°F on upper fluted-tube thermocouples (TC11 and TC12).
19.1	TC12 failure.
19.2	TC11 failure.
19.9	Temperature plateau at 2510°F starts for TC10.
20.4	TC1 failure; upper 2/3 of fuel deformed.
21.3	TC10 failure.
21.7	TC9 failure; beginning of slumping in central pin, slumping accelerates until the eructations; top 1/3 of fuel does not slump.
26.9	First major fuel motion; flowmeters and pressure transducers show dramatic increase in oscillation amplitude; hodoscope shows axial movement of fuel, originating simultaneously 1/3 of the distance from the top and from the bottom of the fuel column. Upward spurt of fuel leaves deficit centered 3 in. above midplane and smaller deficit centered 2-1/2 in. below midplane.
26.9	TC7 and TC8 failure.
30.2	Scram.
31.3	Second major fuel motion; flowmeters and pressure transducers show dramatic increase in oscillation amplitude.

TABLE VII. Comparative Test Times (sec)

Event	L2	L3	L4
First boiling indication	16.4	15.6	13.4
Effective flow cessation	17.3	16.2	14.2
Dryout suggested	∿19	17.5	15.3
Stainless steel melting indicated	20.5	22.0[a]	18.9[a]
First fuel motion indications	22.3 (axial slumping)	∿23[b]	19.0 (radial)
Abrupt fuel motion (axial)	27.7	29.8	26.9
Subsequent fuel motion (axial)	29.5	-	31.3[c]

[a]Fluted-tube thermocouples.

[b]Estimated value of 22.2 sec based upon failure of fluted-tube thermocouple.

[c]After scram.

the order of 0.05 mV (17.5 cm/sec). There is also a possible zero shift of the order of 0.1 mV (35 cm/sec). The same problems in accuracy of flowmeter data exist for L3 and L4. In addition, the void-detector data in L2 could not be quantitatively interpreted, although the void-detector voltage oscillations tended to be in the phase with the void curve derived from flowmeter data. In L3 and L4 the progression of boiling temperatures as indicated by thermocouples along the fluted tube, if the temperatures are taken to reflect boiling, did not agree well with voiding curves from the flowmeter data.

Some information on coolant voiding can also be inferred from the shape of the fluted-tube thermocouple temperature and the loop pressure curves. A typical thermocouple curve is given in Fig. 13, and typical pressure transducer data are given in Fig. 14 (TC10 and inlet pressure-transducer data from L3, respectively). Since the temperatures were measured on the fluted tube and not on the fuel pins, the conclusions about events occurring inside the tube are inferred. The first temperature plateau, at the local sodium-boiling temperature, suggests local or bulk boiling, with a film of sodium on the fluted tube. It is likely that sodium was refluxing down the fluted tube as the sodium films on the fuel pins were drying out.

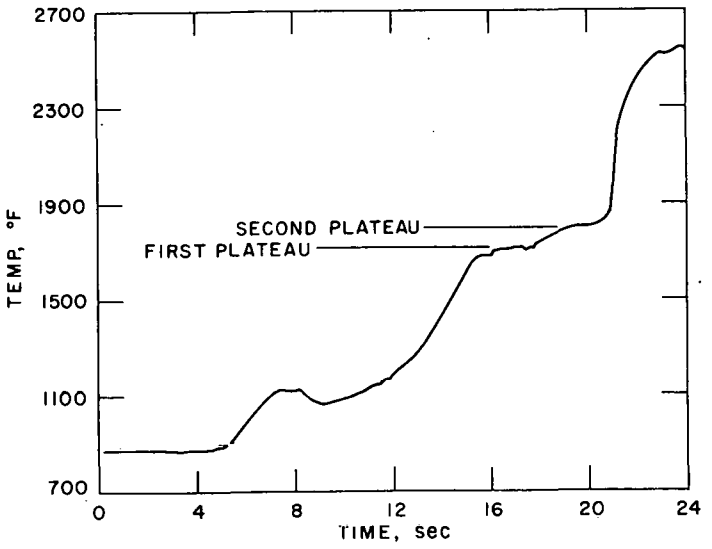

Fig. 13. Typical Data from Fluted-tube Thermocouple.

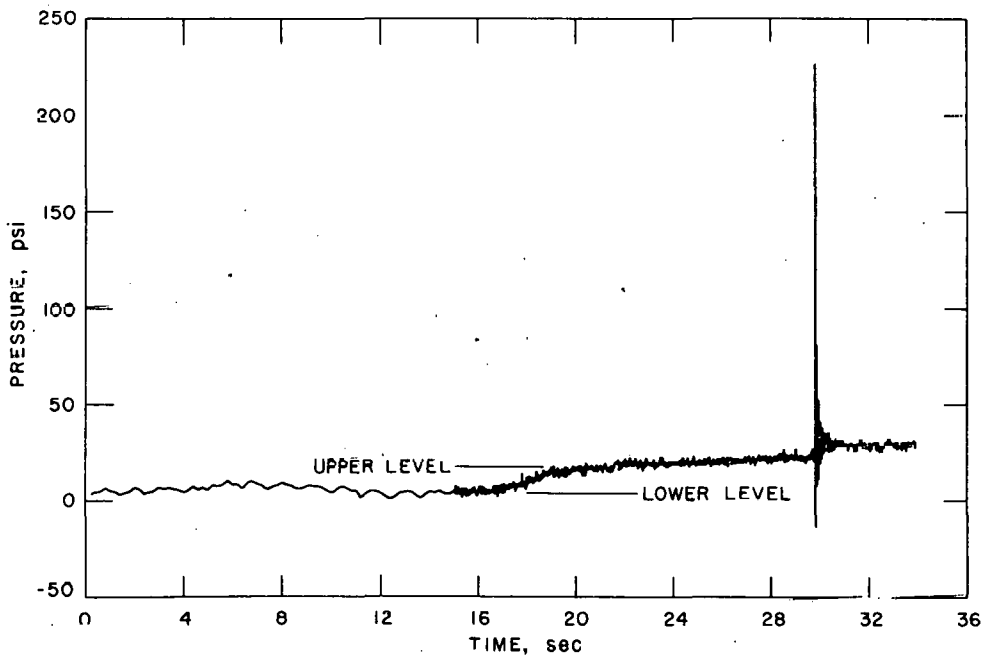

Fig. 14. Typical Data from Pressure Transducer.

The flow signals recorded by the inlet flowmeter were different for the tests with fresh fuel, L2, and the tests for preirradiated fuel, L3 and L4 (see Figs. 10, 11, and 12). The flow in L2 oscillated from 4 to 6 Hz, increasing in amplitude and frequency until it suddenly decreased to a low value. The reduction or sudden decrease in flow has been interpreted as caused by a flow blockage. This flow blockage occurred less than a second after molten stainless steel was detected by the thermocouple in the coolant at the top of the fuel column.

In L3 and L4 the flows oscillated at 3 to 6 Hz, with maximum amplitudes simmilar to those in L2, but with amplitude gradually rising and then falling to a low value, corresponding in time to the detection of molten stainless steel by the fluted-tube thermocouples. Subsequent oscillations were of slightly larger amplitude. They terminated in L4 shortly after central-pin-fuel slumping ended as observed by the hodoscope. There was no quiet period prior to the eructation, although the flowmeter signals tended to die out.

The signals recorded by the upper flowmeter are difficult to interpret. In L2 the oscillations correlate well in frequency, phase, and relative amplitude with those from the inlet flowmeter. They terminated at the same time that the lower flowmeter indicated plugging. Subsequent signals were erratic. In L3 the outlet digital data were irregular. In L4 the outlet data were more regular but did not correlate with the inlet-flowmeter data.

In summary, conclusions regarding sodium-boiling voiding dynamics are very difficult to make. There are strong indications that "one-dimensional" voiding did not occur in the L-series tests. In addition to the complications due to the geometry of the fluted tube and the bundle of seven fuel pins, the average power in the center pin was about 70% of the average power in the outer pins. SAS calculations predict inlet-flow reversal much too early and abruptly in the transient. Thus a two-dimensional voiding model is probably needed to correctly represent the noncoherence in the test section.

3. Dryout and Fuel-pin Failure

Typical fluted-tube thermocouple and pressure-transducer data for a loss-of-flow experiment with preirradiated fuel, either L3 or L4, are shown in Figs. 13 and 14. Note the two distinct plateaus in temperature and the corresponding levels in pressure. There is a gradual rise in both pressure and temperature between about 17.5 and 19 sec. This pressure rise can be attributed to the failure of the fuel pins.

Failure of the fuel pins would release the gas from the pin plena to the loop. The gas would be at a higher pressure than that in the loop plenum and thus would increase the pressure in the loop. Since the saturation temperature of the sodium is a function of the pressure, an increase in loop pressure will cause a corresponding increase in the temperature measured where the sodium is boiling. The calculated pressure rise is approximately that indicated by the loop pressure transducers. The temperature rise based upon the loop pressure rise also matches the

temperature rise indicated by the fluted-tube thermocouples. The experimental data from both experiments L3 and L4 compare favorably to calculated values.

On the other hand, a second temperature plateau was not indicated in experiment L2 by the thermocouple at the top of the fuel column nor was a pressure increase indicated. The calculated pressure rise possible from fuel-pin failure in experiment L2 is much less than that in L3 or L4. Thus the lack of measured rises in L2 is consistent with the calculations performed.

The experimental data from all three experiments do not indicate a sudden release of gas from the fuel pin. There are no evident pressure pulses or abrupt flow perturbations which could clearly result from either plenum gas release due to clad failure or sudden release of fission gas from a melting fuel pin. The signals suggest a gradual release of gas over about 1-1/2 sec, probably with incoherent pin failure, after the coolant channel has been locally voided.

Although no significant difference in voiding dynamics was observed between L3 and L4, the rate of plenum gas release might be expected to be greater in L3 than in L4. This would be due to the larger impedance to gas release from the plenum in L4, which had both a longer length of insulator pellets and a solid Inconel reflector. However, there are significant differences in voiding behavior between the fresh-fuel experiment L2 and the preirradiated-fuel experiments L3 and L4. The flow velocity pattern in L2 contained marked oscillations, suggesting periodic collapse and expansion of vapor bubbles. This pattern was not as strong in L3 and L4. The difference has been attributed to a gradual gas release from the irradiated pins. Sodium voiding seems to be a complex situation involving two-phase flow with sodium refluxing down the fluted tube combined with possible plenum gas release. In addition, the thermal distortion of the fuel bundle is likely with consequent changes in flow channels.

Sodium was found in the plena of three of the seven fuel pins used in the L2 experiment. The presence of sodium suggests that plenum gas was released during the experiment and sodium drawn in as the experiment cooled down. The quantity of sodium was determined by weighing parts with sodium and after cleaning with ethyl alcohol. Posttest examinations of the plenums of pins used in the L3 and L4 experiments can be expected to give similar information.

The time of pin-cladding failure in the loss-of-flow experiments can be expected to be sometime between the start of boiling and the start of clad melting, a period of about 3 sec. The cladding is assumed to fail when the clad strength drops below that necessary to contain the plenum-gas pressure. If the plenum-gas temperature is taken as 1850°F, the upper temperature level indicated by the upper fluted-tube thermocouple gives pressures of 65, 350, and 710 psi, respectively, for L2, L3, and L4. The corresponding circumferential thin-wall hoop stresses based upon a 0.015-in. wall thickness are 460, 2500, and 5100 psi. Comparison to experimentally determined burst pressures for irradiated cladding in Table VIII, and remembering that the strength of stainless steel probably drops suddenly somewhere above 1400°F (the half melting point), implies clad failure in all experiments occurred after clad dryout, when clad

TABLE VIII. Clad Burst Pressures[9]

Temperature, °F	Average, ksi	95% Confidence, ksi
600	18.8	17.7 - 20.0
800	14.8	14.2 - 15.5
1000	13.6	13.0 - 14.2
1200	11.0	10.5 - 11.6
1400	8.4	7.9 - 8.9
1600	5.8	5.5 - 6.2

temperatures are increasing rapidly. Some early failures during burst tests of cladding similar to that of the pins used in the L4 experiment have been informally reported. These failures were attributed to greater-than-expected intergranular chemical attack on the inner surface of the cladding.

In summary, dryout and fuel-pin failure can be based upon experimental data. The first plateau is interpreted as the process of cladding dryout. Near the time the cladding dries out the pins fail, a corresponding rise occurring in measured temperatures and pressures. The second plateau is interpreted not only as continued dryout of the fuel pins but also as drying out of the fluted tube. The second temperature plateau is terminated by a rapid rise to the steel melting point. Shortly thereafter the melting of the fluted tube at some axial location then causes the failure of the thermocouple. Calculations performed indicated that clad melting probably occurred before the complete dryout of the sodium film on the fluted tube. Thus, the temperature rise from the second plateau could be caused by the impingement of molten cladding on the fluted tube. Also, once the cladding and spacer wires are molten, the fuel itself can move radially, for example by pin bowing, and thus hot fuel could contact and melt through the fluted tube.

4. Prefailure Fuel Motion

Fuel motion prior to fuel melting or even clad melting was indicated by the hodoscope in all the experiments. Thermal gradients are expected in the fuel bundle. The fuel itself will be hotter away from the pump and toward the outside of the bundle. The clad and coolant will tend to be hotter toward the center of the bundle. These temperature gradients are due to the combination of power skewing due to the nonsymmetry of the loop, power gradients from self-shielding of the fuel, and overcooling of the outside of the pins. Temperature calculations for the L-series experiments have been performed for undistorted fuel-pin-bundle segments. Temperature differences across the fuel pin of the order of 100°F have been calculated. Inasmuch as the fluted tube does not simulate spacer-wire support of adjoining fuel pins, the outermost fuel pins could deflect outward by thermal bowing and contact the fluted tube along the upper part of the heated length in the direction away from the pump. In fact, the

entire fuel bundle and possibly even the fluted tube could bend. All these deformations could in turn influence the temperature distribution within the bundle. Thus, significant motions are to be expected both during the heat-balance and flow-coastdown runs. Calculation of the deformation could theoretically be done, but such calculations are not at present practical.

During the second L2 transient, the test approaching the loss of structural integrity of the fuel pin, the fuel cluster was observed to bend uniformly toward the pump. In addition, some small variations in the hodoscope data could be interpreted as caused by the temporary bending of a single peripheral pin. The posttransient neutron radiographs indicated some permanent bending of the cluster had taken place. However, the extent of bending was small and no sign of pin damage was detected. Cooling of the cluster could be expected to return it to near its initial configuration. The presence of some permanent bending seems more likely due to configuration changes allowed by mechanical tolerances than plastic deformation.

In contrast, the final L2 transient, the loss-of-flow simulation, gave no indication of overall cluster bending. Thus it seems that the motions observed during the second transient left the bundle in a configuration for which differential thermal expansion could not cause further distortion. Some small variations occurred similar to those in the second transient. Those in the final transient appear to be a temporary shift of the pin farthest from the pump. The greatest movement was in the top third of the pin. Duration of the displacement until recovery to its original position was about 2 sec.

In the L4 experiment there was also some early movement in the cluster. Bowing commenced early in the transient, evidently before the preheat power level ended. Both a coherent and incoherent squirming of individual pins in the cluster was detected. Because of an increase in rapidity of fuel-pin motion, the cladding was probably either molten or very soft about 1-1/2 sec prior to apparent failure of the fluted tube. Axial fuel expansion was observed at the same time as the fuel pins bowed. The entire bundle bent abruptly away from the pump at about the same time molten steel was detected by fluted-tube thermocouples. The movement was large enough to indicate that fuel was leaning against the outer wall of the adiabatic holder, near the primary vessel. This movement took about 1 sec to complete. During the 3-sec period from this motion until the start of fuel slumping, only minor movements took place. The analysis of the L3 hodoscope data is incomplete. Nevertheless, the cluster underwent some radial motion in the 6 or so sec preceding the fuel eructation.

5. Molten-clad Dynamics

Clad motion cannot be directly observed during an experiment. Some information can be derived from the thermocouple and flowmeter data. From the experimental data the time of failure of various thermocouples can be determined. The failures imply melting of the thermocouple leads after melting of the adjacent fluted tube. In L2 the end of flow oscillations implies a flow blockage due to freezing of steel plugs in the coolant

channels. An indication of the extent and location of the blockage is given by the remaining ability of the pressure transducers to record pressure pulses and of the flowmeters to record flow perturbations; a signal from these instruments implies an open passageway from the source of the signal. The hodoscope does not provide any data on clad motion. Comparison of pretest and posttest neutron radiographs gives some indication of final steel location, but the radiographs are more sensitive to fuel and their value is in providing tentative information prior to posttest examination. Posttest examination is the only reliable method of determining steel location after the experiment is completed.

Only the L2 experiment has undergone, at this writing, complete posttest examination. There are only preliminary posttest examination results for L3 and L4, and no conclusions on steel motion during these two tests can be drawn. The test section for the L2 experiment has been cut into 4-in.-long sections and the sections cut in half longitudinally. The pieces were heated to 125-150°C to melt out the sodium. The sodium remaining on the pieces was reacted with ethyl alcohol. The pieces were then rinsed with alcohol, dried, and examined. Then final sectioning and examination were performed. Figures 15 and 16 show the location of the various cuts.

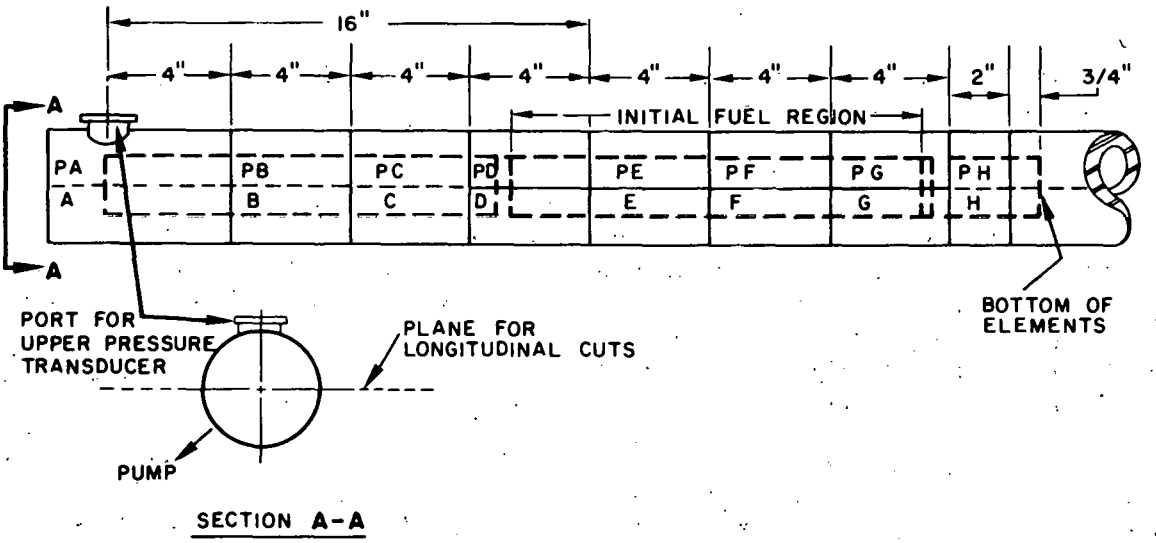

Fig. 15. Cutting Scheme for L2 Test Section.

The upper steel plug (see Fig. 17), about 1/4 in. thick, was located in the region of the upper insulator pellets. Steel in this plug appeared to be solid, although a channel apparently existed along the periphery of the fuel cluster. At this point the steel melted through the fluted tube (the inner wall of the adiabatic holder) but did not melt the outer wall of the adiabatic holder. In fact, the outer wall was intact, and was easily separated from both the loop and the aggregate of melted fuel and stainless steel.

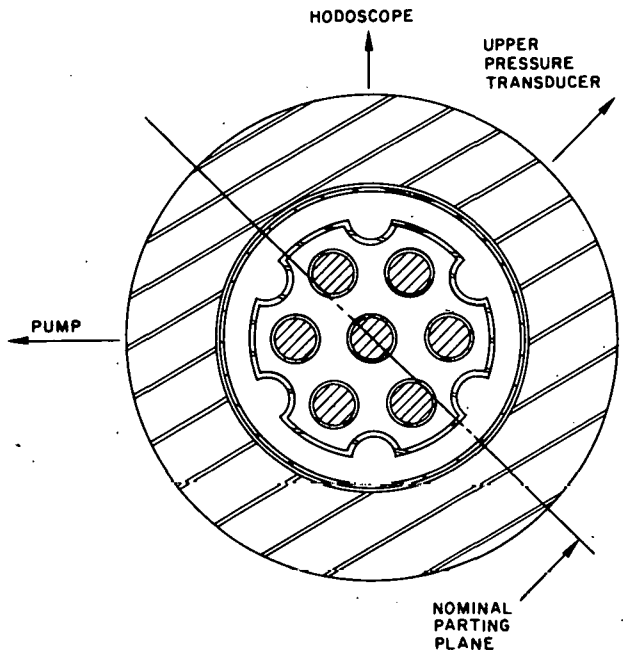

Fig. 16. Orientation of Longitudinal Cut.

The lower plug (see Fig. 18) was an irregular solid block of steel about 1-1/4 to 1-1/2 in. thick. The location was again near the insulator pellets, extending upward about 1/4 to 1/2 in. into the fuel region and down from there. The lower part of the plug had the appearance of material that froze when it splattered on a colder surface or dripped into a colder fluid (see Fig. 19). This lower part was not bonded to the fluted tube. Note the walls of the adiabatic holder in the region of the plug were separated by a steel ring. Above the ring the fluted tube was melted through, and steel filled the space out to the outer wall of the adiabatic holder. Below the ring the fluted tube was intact, but some sodium was found in the space between the walls. The outer wall could not be removed from the primary vessel. Thus a solid inlet plug of steel inside the primary vessel existed, although some voids existed in the midst of the steel.

Another source of information on clad motion is the flowmeter data. The L2 experiment was the only one with strongly pronounced flow oscillations measured by both flowmeters. The oscillations of both the upper- and lower-flowmeter data stopped at the same time, 21.2 sec. The blockage probably occurred before the fluted tube melted. Thus, the blockage can be attributed to the freezing of molten clad. Both the upper and lower blockages seem to have formed at the same time.

A cross section at low magnification through the lower plug is shown in Fig. 20. The molten steel evidently formed the plug in two stages. The cladding and spacer wires melted first and flowed downward to freeze among the bottom parts of the fuel elements. On the basis of the reduced molybdenum content found in the frozen steel, some of the Type 304 steel from the fluted tube must have melted at the same time and mixed with the Type 316 steel of the cladding and spacer wires. The fuel then moved downward and in collapsing melted more of the fluted tube. When the fuel reached the frozen steel, it remelted the steel and displaced molten steel upward and sideways to freeze on the outer wall of the adiabatic holder. The molten fuel also caused the steel blockage beneath it to remelt and flow downward as a second flow into available openings or channels.

The eructations in L2 were recorded on both the upper and lower flowmeters but not on either pressure transducer. The eructations in L3 and L4 were recorded on both flowmeters, but only at the inlet pressure transducer. Both the lower flowmeter and the lower pressure transducer

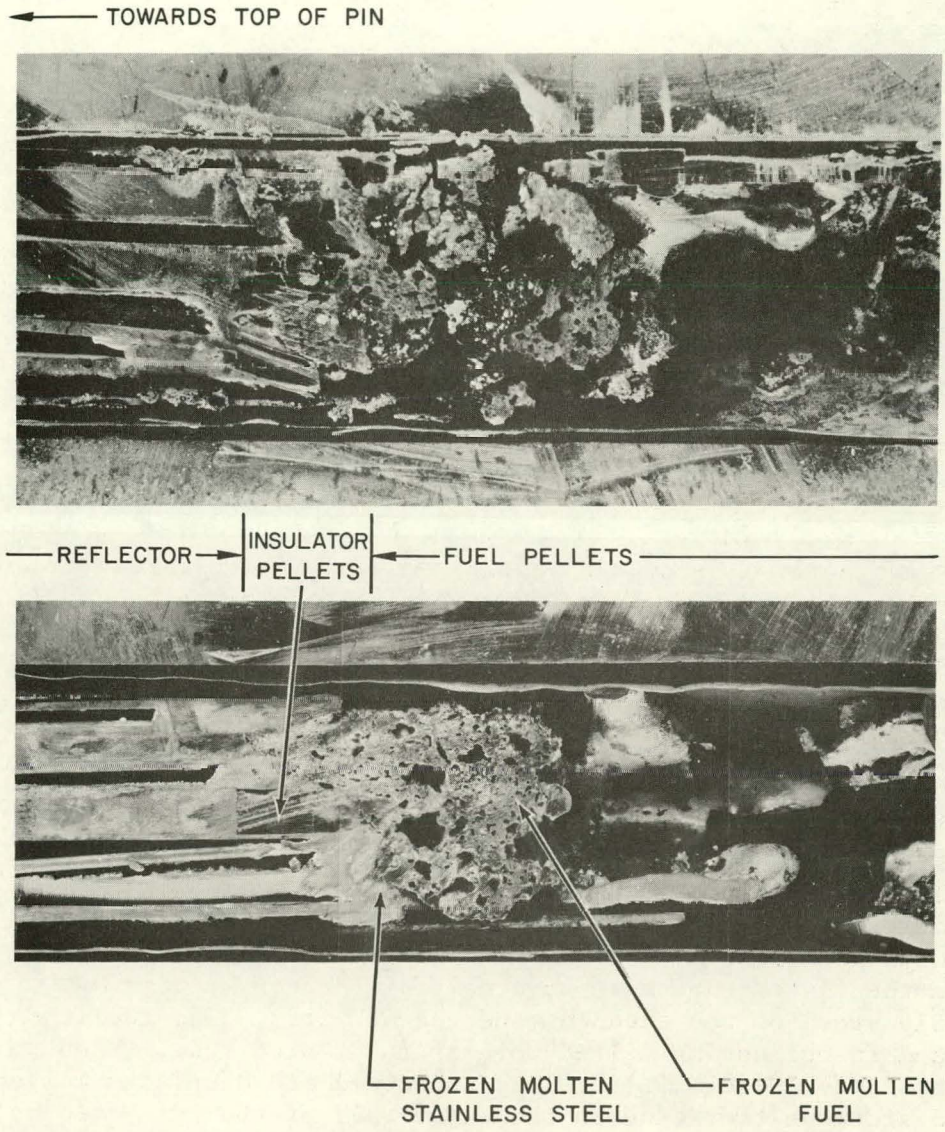

Fig. 17. L2 Posttest Examination - Upper Blockage (∿1-3/4 X).

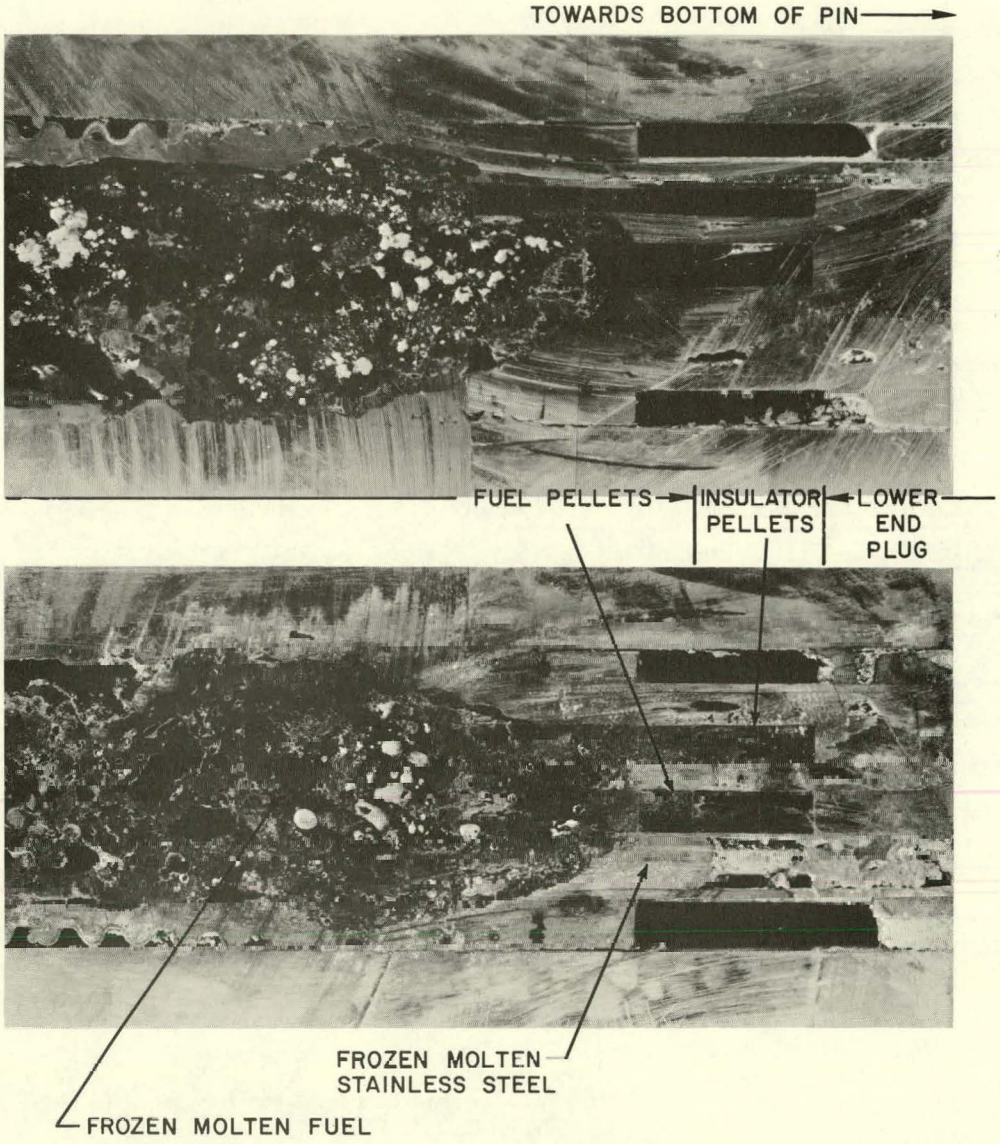

Fig. 18. L2 Posttest Examination - Lower Blockage (∿1-3/4 X).

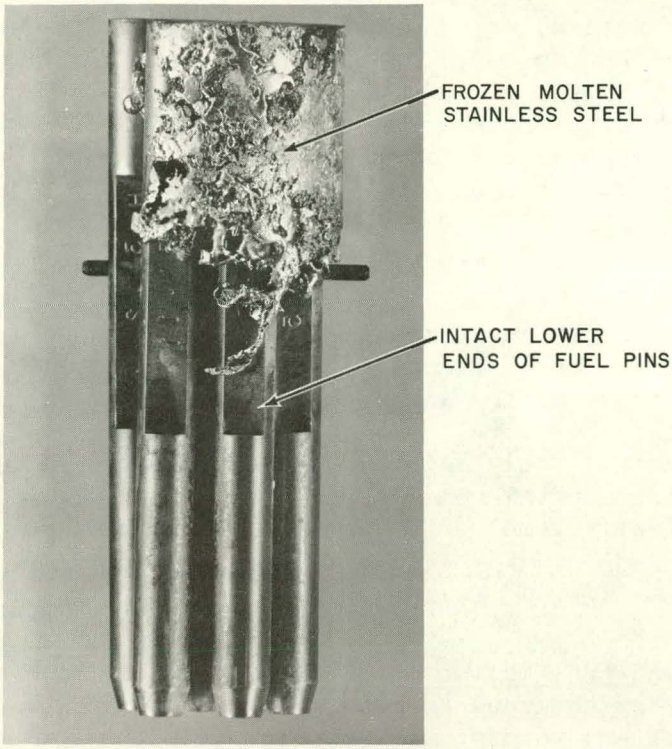

Fig. 19.
L2 Posttest Examination - Bottom of Fuel Bundle (∿2 X).
MSD Neg. No. 165588.

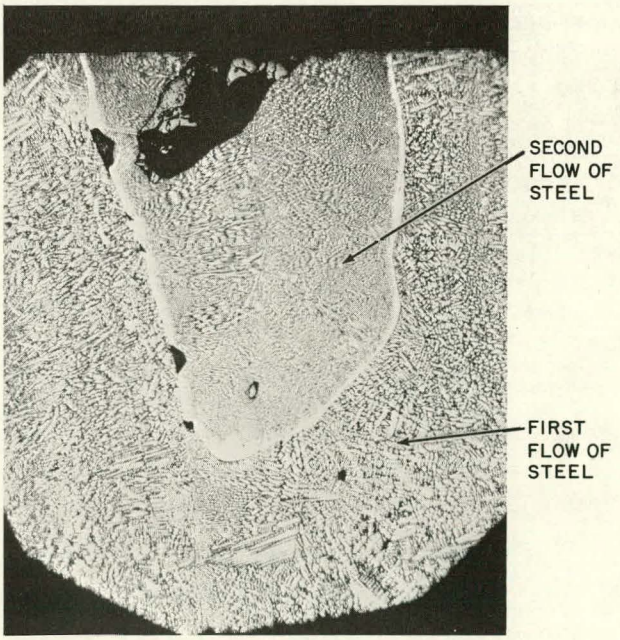

Fig. 20.
L2 Posttest Examination - Lower Steel Plug (100 X).
MSD Neg. No. 166097.

were below the test section. The upper flowmeter measured flow within the fluted tube. The upper pressure transducer was above the adiabatic holder, the outer wall or convoluted tube having ended. Pressure signals reached the transducer through an opening in the fluted tube. The lack of coherent pressure-transducer and flowmeter signals is attributed to partial plugging, which isolated the pressure transducer from the source of the pressure transients accompanying the eructations.

6. Molten-fuel Dynamics

Significant differences were observed between the fuel motion in L2 using fresh fuel and the fuel motion in L3 and L4 using preirradiated fuel. In experiment L2, the dominant motion was a complete collapse of the fuel bundle followed by an eructation several seconds later. In experiments L3 and L4 the fuel moved axially only slightly, apparently not undergoing any large-scale slumping for several seconds until the fuel was ejected toward the ends of the fuel column.

(a) Experiment L2

The first prominent fuel motion in L2 after clad failure was a collapse of the upper part of the fuel columns in the cluster. The collapse was initiated by an apparent voiding of fuel from the location of the center pin about 2 to 3-1/2 in. above the midplane. The fuel voiding progressed at this level to the side toward the pump, implying a loss of fuel from at least the pump-side peripheral pin. This is an unexplained event since this pin should be the coolest pin in the bundle. A loss of fuel away from the pump would be expected to occur first. The material from this voided region dropped downward without any indication of any upward motion. The downward motion left the pellets above this region unsupported. As expected, the voided region began to be filled with fuel as the upper region began to lose fuel. The upper pump-side fuel then collapsed entirely. The observable collapse started at 22.31 sec and lasted until 23.7 sec. Almost all the fuel in the upper third of the cluster collapsed. Detailed hodoscope-time plots indicate that the fuel completely left that region. The region also can be inferred to be void of sodium and steel. The rate of fall was of the order of 10 cm/sec. The fall could be either a flow of molten, melting, or solid material, or a combination thereof, under gravity into a region bounded by cooler solid material. All the fuel motion to this time occurred within the fluted tube.

Following the first collapse was a quiet period of nearly 4 sec. No major change in the location of the fuel took place during this time interval. However, local turbulence was noticed on the side of the cluster away from the pump, about an inch below the top of the intact fuel. By the time the quiet period ended, a small voided region had grown upward.

At 27.7 sec (transient time), about 11.3 sec after the initiation of boiling, a sudden fuel motion took place. Fuel moved from the midregion in all directions, with most of the fuel moving upward and less spreading laterally outward or moving downward. The fluted tube was penetrated on the side away from the pump at a point about two-thirds of

the way up the original fuel column. The extent of fuel motion upward was apparently impeded by either the fuel which had not slumped or frozen molten steel between the upper parts of intact fuel pins. The hodoscope detector channels above the original position fuel column did not indicate fuel at any time during the transient, so fuel was not ejected above the top of the original fuel column. The upward motion was followed by the collapse of the ejected fuel. The fuel fell back within a second of the start of the motion. The rate of fall averaged about 25 cm/sec.

Prior to scram, one more major eructation and collapse occurred similar to the first. During the second eructation a large amount of fuel became splattered near the primary vessel as the fluted tube gave way. All hodoscope activity ceased with reactor scram. There was no evidence that the eructation and collapse sequence would not have continued if reactor power had been maintained.

Posttest examination confirmed that substantial fuel melting and movement occurred. Most of the fuel appeared to be concentrated in a region approximately 5 in. high, with its bottom nearly coincident with the bottom of the original fuel column. Much of the fuel holder was destroyed in this region, but the end fittings of the pins were substantially intact. A small amount of fuel appeared to be concentrated near the top of the original fuel column. The top structure of the pins was substantially intact, with only a small amount of upward movement of the reflector pieces. Little or no fuel was apparent outside the test-section region (see Figs. 17 and 18).

When the fuel slumped, it was apparently partly molten or near its melting point. The fuel after collapse was molten as it mixed with the steel at the bottom of the test section. During posttest examination the fuel was observed in the lower fuel plug to consist of unmelted pellets, partially melted pellets, and frozen melted pellets (see Fig. 21). The partially melted fuel was quite porous and swollen with voids which could have been generated by gas pressure. One such piece of incipient melted fuel was determined to have a 47% areal porosity compared with the 7 to 13% areal porosity of fuel in cooler locations.

Steel was found at various locations in the fuel. Melted steel was found to have penetrated into the interior of an unmelted fuel pellet by flowing through and filling cracks in the fuel. The frozen molten fuel in both the top and bottom plugs contained particles of metal, apparently stainless steel, dispersed within it, although regions without metal particles also were present. The particles occurred in regions observable as light colored bands in the fuel. An example of the particles is shown in Fig. 22 (bottom) and of the light colored bands in Fig. 22 (top). As indicated in the discussion of molten-clad dynamics, the collapsed molten fuel caused the steel blockage beneath it to remelt and relocate. Molten steel trapped by the molten fuel was less dense than the molten fuel. The steel would then rise up through the molten fuel. As the molten steel rose, it dispersed into droplets. The columns of droplets show up as light colored bands in the photographs.

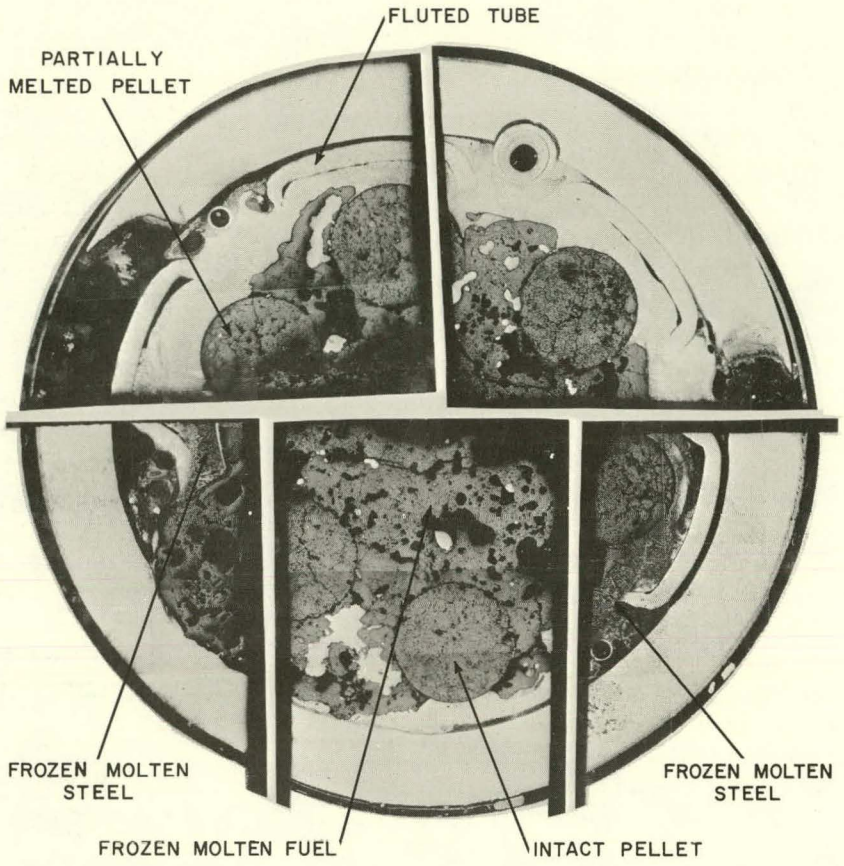

Fig. 21. L2 Posttest Examination - Transverse Section of Lower Blockage (3-1/2 X). MSD Neg. No. 167677.

(b) Experiment L3

Preliminary processing of the hodoscope data has been completed. Fuel dispersal started at 29.8 sec (transient time) or about 14.2 sec after the initiation of boiling. The dispersal was an eructation that voided much of the upper half and part of the lower half of the fuel region. The center of the extensively voided region was about 1 in. above the original fuel midplane. Most of the displaced fuel moved up, but some was also forced down. There was no sign of fuel slumping or of reentry after the dispersal.

The most prominent features in the radiographs (see Figs. 23 and 24) are the extensive removal of fuel from the midregion of the column, and the displacement of fuel upward past the original top of the column. The bulk of the fuel that was displaced upward out of the original fuel region was concentrated in the space 3 in. above the original top of the column.

Since the region from the original top of the column down to a level about 2-1/4 in. below appears as a solid zone of fuel in the radiograph, and since fuel did move up out of the column, it follows that fuel was displaced to fill in this region at the top of the column from the voided central region.

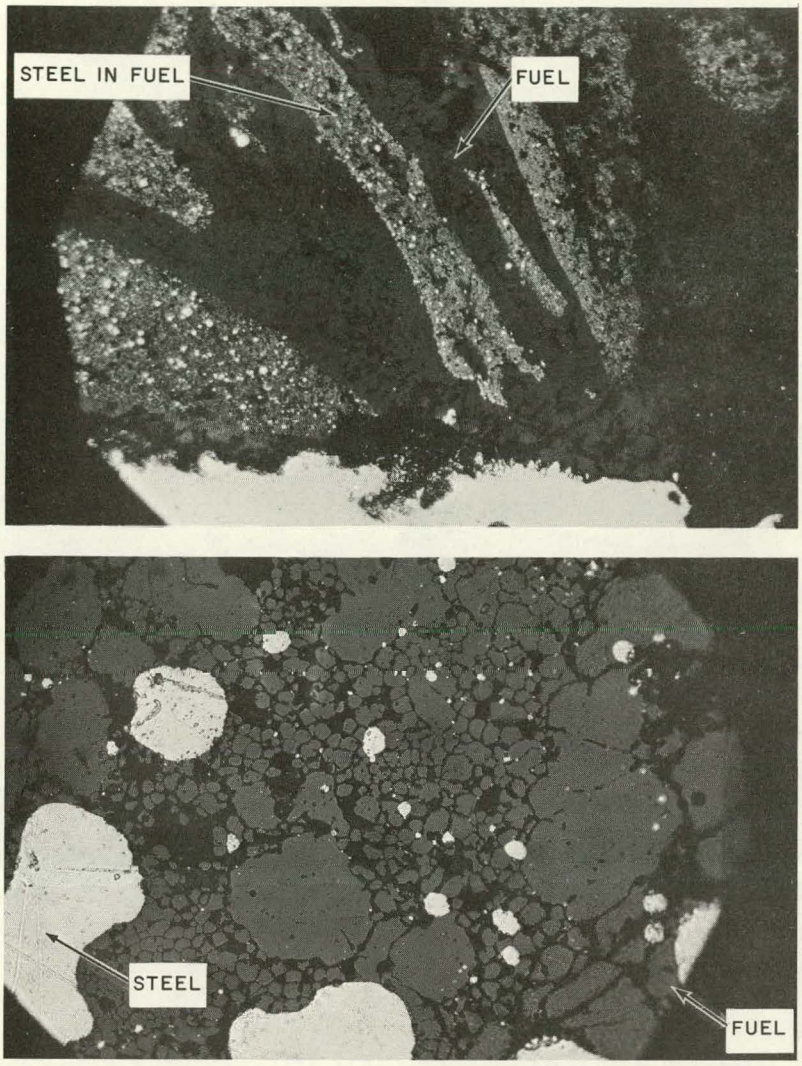

Fig. 22. L2 Posttest Examination - Metallic Particles in Fuel (Top 250 X) (Bottom 500 X). MSD Neg. No. 166433.

The bottom 4 in. of fuel column contains a few small voids according to the radiograph. Some fuel movement apparently occurred in this region, but the amount was relatively small compared to that involved in the upward movement. The expulsive forces, while mainly moving fuel upward, also pushed some fuel downward.

Posttest examination of L3 has been started, but is not complete. Preliminary examination showed fuel plugs at the top and bottom in the same locations as shown by the radiographs.

(c) Experiment L4

Initially the fuel pins in the L4 test moved toward the pump until about 2 sec after boiling initiation. This was followed by

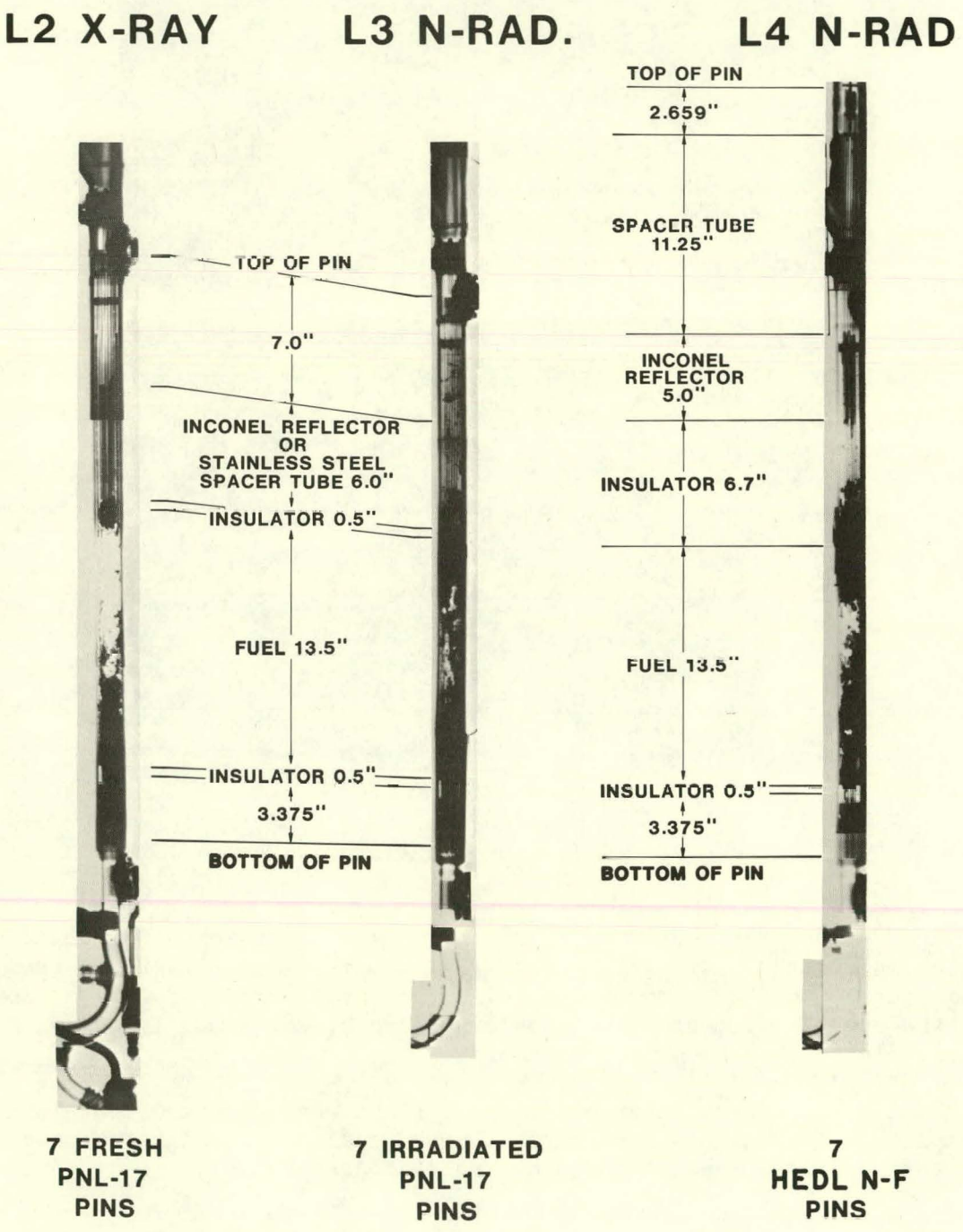

Fig. 23. Posttest Radiographs. ANL Neg. No. 900-3329.

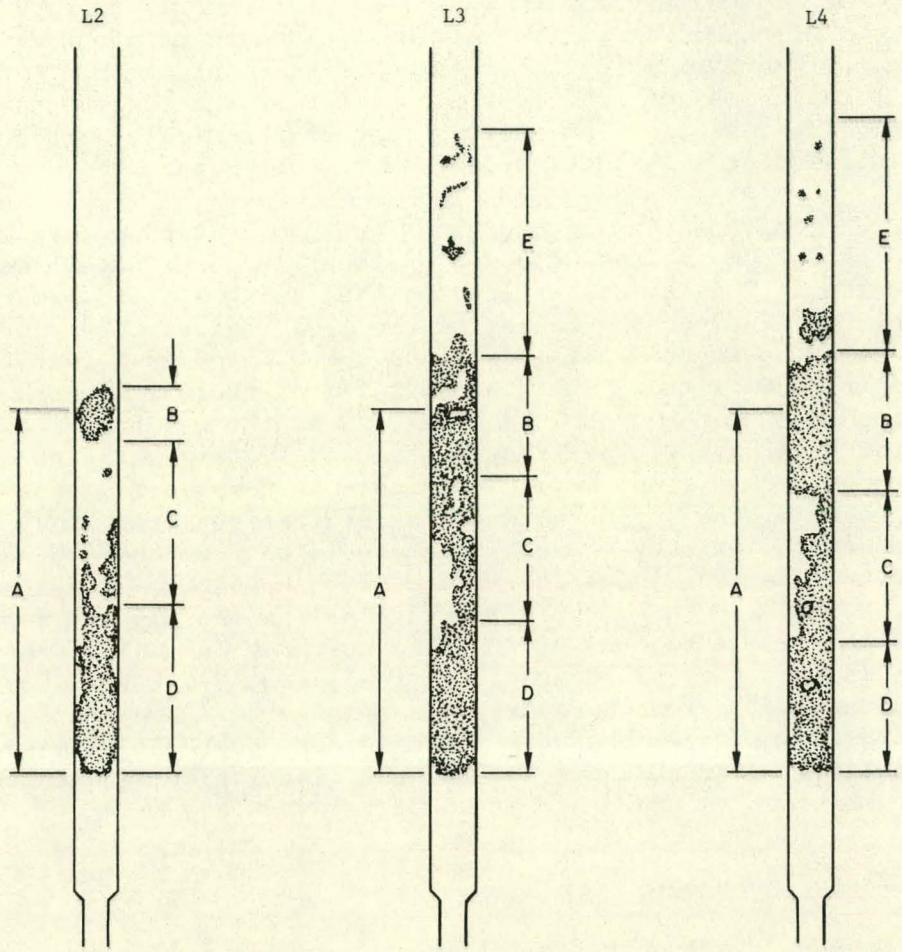

A. Original Fuel Column.

B. Concentration of Fuel and Steel Near the Top of the Original Fuel Column.

C. Region Substantially Void of Fuel.

D. Concentration of Fuel and Steel Near the Bottom of the Original Fuel Column.

E. Fuel or Steel above Top of Original Fuel Column.

Fig. 24. Interpretation of Posttest Radiographs.

pin motion away from the pump, which continued until, at 18.9 sec (5.5 sec after the initiation of boiling), there was a rapid motion of the fuel through the fluted tube and up to the test-section wall. The thermocouples located on the side of the fluted tube away from the pump indicated that the melting temperature of stainless steel was reached at this time; the fluted tube failed 0.2 to 0.3 sec later. A gradual spreading out of the lower portion of the fuel began at about 22 sec, indicating that some slumping had started in at least one pin. At 25 sec there was a rapid loss of fuel from the center of the fuel bundle. This was probably the result of the melting away of the middle portion of the central pin, leaving a stalactite-stalagmite configuration.

The most prominent feature of the hodoscope data was the eructation which occurred at 26.9 sec or about 13.5 sec after the initiation of boiling. This event resulted in fuel being ejected upward and a replenishment of fuel at the center of the fuel region. There was no sign of fuel reentry up to the time of reactor scram. The fuel that eructed originated from two sites. One was about 1/3 of the way from the top of the fuel column, and the other was about 1/3 of the way from the bottom. In the first region, fuel was removed extensively from both the middle and the side opposite the pump, while less fuel was removed from the pump side. Over the length of the region between the eructation sites, fuel moved outward toward the primary vessel. The expulsion from the two sites (one just below and one just above the middle of the cluster) was essentially simultaneous, and led to accumulations of fuel in the top and replenishment of fuel in the middle regions of the fuel column. The major features in the radiograph are the upward displaced fuel, some 3-1/2 in. above the original upper fuel column boundary, and a large void about 1/3 of the way down from this same upper boundary. Preliminary posttest examination of L4 showed results similar to those for L3, that is, fuel plugs at the top and bottom in locations as shown by the radiographs.

7. Flow Blockages

Posttransient operation of the pump while the sodium in the loop was still molten indicated little or no flow of sodium in all three experiments. The posttest neutron radiographs indicated the presence of deposits of fuel and steel at both the top and bottom of the original fuel region. The posttest examination of L2 showed a relatively solid plug of fuel resting on a thick stainless steel plug at the bottom of the fuel region. Another relatively solid, but smaller, plug was at the top, resting against a partial steel blockage. The fuel in the lower plug was solid at the bottom, with a porosity increasing toward the top. The upper plug was porous, with a visible channel or passage through the plug.

The sequence of events in L2 suggest that the fuel was not ejected upward into a region where it could form a stable plug, that is, the upward ejected fuel would fall back down. On the other hand, the molten fuel at the bottom could melt the surrounding steel and then freeze to form a solid crust of mixed oxides, thus completely blocking the loop inside the primary containment vessel.

Hot fuel melted through the fluted tube (the inner shell of the adiabatic holder) in each experiment. The molten fuel in some cases melted the outer wall of the adiabatic holder. There was no evidence that the inner surface of the loop primary vessel had been melted. Fuel froze in some cases to either wall of the adiabatic holder or to the primary vessel. In some places where the outer wall of the adiabatic holder was not melted away, it was apparently welded to the primary vessel. It should be noted that sodium filled the gap between the primary vessel and outer wall of the holder at the start of each experiment.

Posttest examination of L2 showed that although the height of the sodium in the two legs of the loop seemed to be the same, the large voids among the elements in the pin plenum region imply that sodium had flowed down through the upper blockage to fill the space beneath. Sodium flowing down had access to the space between the walls of the adiabatic holder as well as the plenums of the test fuel elements. The sodium could not move through the blockage at the bottom.

The extent of blockage in L3 and L4 will be determined by detailed posttest examination. Preliminary examination of L3 and L4 indicate possible fuel blockage both at the top of the fuel column and a few inches above the bottom of the fuel column.

In L3 and L4 the fuel remained dispersed upward for 2.5 sec and 3.3 sec after the eructation (prior to reactor scram). In L4 there were some indications that fuel fell down after scram. Evaluation of the final disposition of the fuel in L3 and L4 will have to await completed posttest examination.

All experiments indicate that fuel froze near the ends of the fuel region. Contributing to this is the fact that the fuel is at a lower average power when collected at the ends of the fuel region because of being shielded by the dysprosium filters which provide prototype axial power shaping. In addition, a large block of fuel would have significant self-shielding.

In all three loss-of-flow experiments, using the data presently analyzed, a complete blockage due to fuel and clad must be assumed. The solidified fuel blockage is solid enough not to be cooled by flowing sodium to any significant extent.

IV. INTERPRETATION OF TEST RESULTS

The L-series tests are of particular interest in determining the effects of fission gases on fuel motion, the conditions leading to fuel motion, and the speed and direction of fuel motion. The tests provide an experimental evaluation of fuel motion in order to verify and improve fuel-motion models developed to model fast-reactor accidents. The experiments will be compared to the SAS model in the Appendix. The tests results have been summarized in Sect. III. This section will interpret the results to provide the best possible mechanism to explain fuel motion.

A. Fuel Collapse

The fuel in L3 and L4 did not collapse after clad melting as it did in L2. The difference in behavior was not surprising since the behavior of preirradiated fuel could be expected to be different from that of fresh fuel. The difference in behavior can have several possible causes.

The first possibility is that the fuels in L3 and L4 were cooler than in L2. Cooler fuel would be less plastic and less fluid in behavior. But significant differences in temperature between the experiments seem unlikely. The power levels were similar in all three experiments. Cooling by radiation and conduction to the adiabatic holder should have been similar for all three experiments. If cooling was not sufficient to keep the fuel in L2 from collapsing, it should not have kept the fuel in L3 and L4 from collapsing. Calculations for heat transfer by radiation give a wide variation in power loss from the fuel, depending on the surface temperatures and emissivities assumed. A large rate of heat transferred would cause a rapid rise in fluted-tube temperatures, leading to the melting of the fluted tube within a few seconds. Similar conclusions result from calculation of heat transfer by convection to the fluted tube. Such a rapid failure of the fluted tube was not detected. Cooling of the fuel by sodium-vapor streaming was also calculated and found insufficient to explain a significant temperature drop. Calculations based on the assumption of no flow blockages and considering the relative value of density, specific heat, and velocity of liquid and vapor sodium lead to the conclusion that an unreasonably high temperature rise of the vapor would be necessary to cool the fuel.

Another possibility is that the flowing sodium vapor could levitate fuel particles. But it seems unlikely that the vapor velocity, gravity forces, and fuel-particle-size distribution could be just right to hold the fuel in place for the several seconds necessary to explain the non-collapse of fuel in L3 and L4.

The possibility exists that enough fission gas remained in the fuel to form a foam or a mixture of solid or liquid, and gas. The foam or bed of particles could be stable with the gas release balanced by the influx of vaporizing sodium or with the coalescence and draining of films balanced by turbulent creation of foam. Again the long stable time needed seems to make this possibility unlikely.

During the L-series experiments the fuel temperatures rose rapidly and the fuel had large thermal gradients. The temperature gradients can cause thermal stresses which can lead to the fuel cracking and possibly to plastic deformations of the fuel. On the other hand, the high temperatures can cause resintering of the fuel, with healing of the cracks, or even cause melting of the fuel, with subsequent refreezing of the fuel in the cracks. It is likely that the fuel in L2 collapsed with the pellets effectively intact, that is, the fuel column just fell apart in pieces of fuel only partly melted once the cladding melted. The fall of the separate partially melted pellets or pellet fragments could account for the slow slumping. On the other hand, the fuel pellets in L3 and L4 could have been relatively intact. In particular, the equiaxed regions created during irradiation could have formed a dense, strong column. The

fuel in L3 and L4 then would either bow as an intact column or break apart into lengths of sintered pellets. Noticeable collapse would then be caused by fuel melting through a large section of the pin cross section and flowing downward between the nonmolten fuel pellets.

Recent out-of-pile experiments did not show evidence of gross fresh fuel cracking upon rapid electric heating. During the tests, molten fuel was ejected from the center of the fuel pellets through the gaps between pellets and cracks in the pellets. Total breaking up of the pellet was not observed. In addition, dry transparent-capsule experiments performed in TREAT demonstrated that a column of fresh fuel slugs broke apart into separate fuel slugs.

What seems most likely is that the irradiated fuel swelled as it heated, that is, the gaseous and volatile fission products caused a volume increase in the fuel. The pellets, then being of a greater effective diameter, were unable to collapse as readily inside the fluted tube as did the fresh fuel. The irradiated fuel prior to melting is thus probably in the form of swollen fuel pellets occupying roughly the same volume as the original fuel bundle.

B. Fuel Eructation

The most noticeable fuel motion in all three experiments was an abrupt upward motion of the fuel. This occurred twice while L2 was at power, once during L3, and once while L4 was at power and again shortly after scram. All of the events at power were similar in that they occurred within approximately 150 msec and originated in that portion of the central fuel region, where the fuel concentration was highest. The L4 eructation originated simultaneously (or almost simultaneously) at two sites, one above and one below a previously formed central void. Possible differences in speed, timing, and coherency between the eructations in the experiments are still being investigated.

The conditions under which fuel motion begins cannot directly be answered by the experimental data. The only reliable experimental indication of fuel motion is the hodoscope. The experimental data from test-section instruments do not directly indicate the state of the fuel at any time nor do they reveal the cause of the fuel motion. All three experiments have been analyzed using SAS/SLUMPY. The calculations predict the temperatures of the fluted-tube thermocouples quite well up to the time the temperatures rapidly rise to the stainless steel melting point. The calculated temperatures in the fuel thus can be expected to be accurate up to the time the fluted tube dries out. The slumping criteria used in the code were half melting of the first node in the unrestructured fuel for preirradiated fuel and approximately 95% areal melting in fresh fuel. These criteria predicted fuel motion at a time earlier than that detected by the hodoscope.

On the other hand, the rate and direction of fuel motion can be determined experimentally by analysis of the hodoscope data. The fuel in L2 collapsed downward at a rather slow rate compared to free fall, of the order of 10 cm/sec. The fuel in L3 and L4 did not collapse as in L2.

Some of the central fuel in L4 did move slowly downward prior to the eructation, but fuel above was left in place. The fuel in L2 was projected upward with a velocity of about 50 cm/sec. The fuel in L3 was projected upward with a velocity of at least 50 cm/sec, whereas the fuel in L4 had a velocity of approximately 100 cm/sec. The previously voided region in L4 was refilled with fuel to about the same density as before slumping from sources both above and below the voided region.

Preexperimental calculations indicated that the preheat and flow-reduction phase of the experiments leaves the fuel in each experiment with roughly the same average energy density. Thus it is instructive to compare rough calculations of energy density based upon the adiabatic heating of the fuel for L2, L3, and L4; results are tabulated in Table IX. Of

TABLE IX. Increase in Average Fuel Energy Density (J/g)[a]

Event	L2	L3	L4
Dryout suggested	320	120 to 440	190 to 400
Stainless steel melting indicated	530	910[b]	810[b]
First fuel motion	940	1060[c]	830
Abrupt fuel motion	1950	2140	2190

[a]Adiabatic conditions assumed from time of cessation of flow (J/g of fuel).

[b]Based on temperatures of fluted-tube thermocouples.

[c]Estimated value.

interest is the agreement of values of the average fuel energy density, in particular, at the time of the abrupt fuel motion in L3 and L4. Note that the average fuel energy density for first fuel motion in L3 and L4 bracket that in L2. This suggests a similar model might be found to fit the data from all three experiments.

In fact, the shorter time and smaller energy between collapse and eructation in L2 as compared to the times and energy between initial fuel motion and eructation in L3 and L4 could be attributed to poorer heat transfer from the center of the larger mass of slumped material in L2, allowing higher temperatures to be reached.

The most plausible ejection mechanism is a local vaporization of stainless steel. The posttest examination of L2 showed steel dispersal in fuel which had been molten. Estimated curves of stainless steel and UO_2

vapor pressure[11] are plotted in Fig. 25. The significant vapor pressure of stainless steel above the melting point of mixed oxide suggests that trapped stainless steel in the fuel could have vaporized and provided the driving force for the fuel eructations. This could have occurred before significant fuel vapor pressure formed.

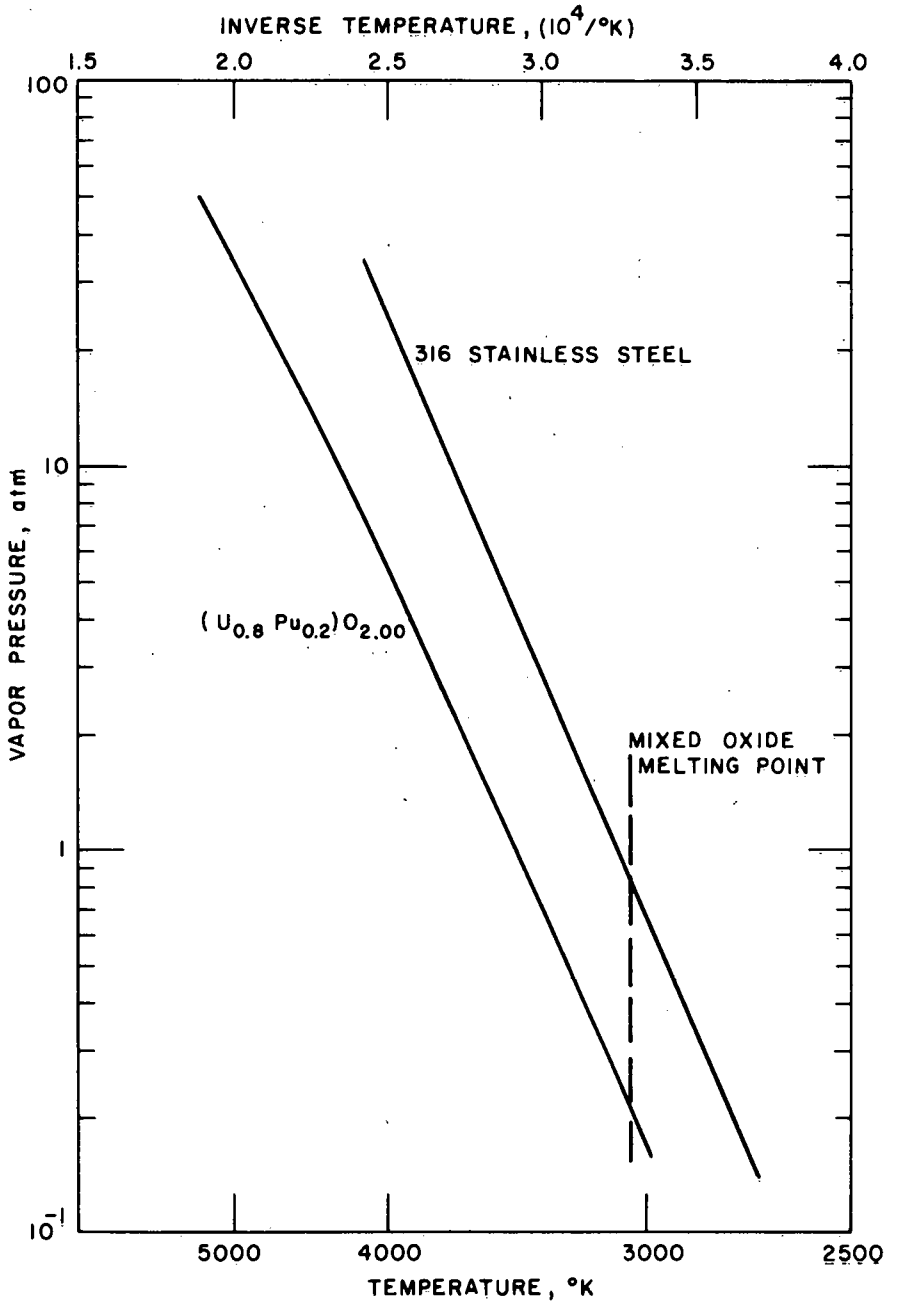

Fig. 25. Vapor Pressures of Stainless Steel and Mixed Oxide.

Posttest analysis of the small metallic particles within the fuel could not distinguish between the Type 304 and Type 316 stainless steel although iron, chromium, and nickel were detected. In several instances the chromium was found to be less than typical by 20 to 50%. The mechanism for this chromium depletion has not been clarified, but it does not seem likely, based upon the vapor pressure of the stainless steel components that preferential distillation of chromium was the cause.

There is an added variable in L2: the void detector. The void detector contained two thick strips of nickel in the adiabatic holder which could act both as a heat sink and mix with the stainless steel and fuel. Mica, which could decompose forming water vapor, surrounded the void detector. But the mica should have decomposed long before any eructation took place.

C. Effect of Fission Gases on Fuel Motion

Part of the fission gas in the preirradiated fuel pins used in L3 and L4 was released from the fuel during irradiation and was in the fuel-pin plenum. The remainder of the fission gas in the fuel is found primarily in the outer part of the equiaxed region and in the unrestructured region. The current conclusions based upon experimental data are that the plenum gas does not directly influence fuel motion, that the data are presently insufficient to determine the influence of the fission gas in the fuel, and that fission-gas effects are not required to explain the fuel dispersal.

A rapid release of plenum gases was not detected through any abrupt perturbation of flow or pressure in any of the three experiments. A gradual gas release over 1-2 sec can be inferred from the experimental data to have occurred when the cladding failed. The cladding probably failed shortly before it became molten. Thus, the release of plenum gases could have influenced the extent of clad plugging, that is, the release of noncondensible gases could have spread out the molten clad, causing it to move radially and freeze on the fluted tube (or the primary vessel) rather than move axially and freeze near the ends of the fuel column. Thus, larger openings or passages through the clad would be left after it froze. This is a hypothetical explanation for the difference in apparent clad plugging prior to fuel motion in the unirradiated and preirradiated tests. A lack of a steel plug would allow sodium-vapor streaming to influence fuel motion. In summary, the release of plenum gases apparently may indirectly influence fuel motion by changing the distribution of frozen clad.

Results of out-of-pile experiments in MSD at Argonne and analysis based on other in-pile experiments performed in TREAT indicate that the fission gas in the fuel will be essentially 100% released from the fuel grains just below the fuel melting point during a loss-of-flow experiment. The gas is released over a period of approximately 3 sec. Apparently most of the gas will be released prior to the detection of fuel motion, but enough gas will remain in the fuel to cause significant fuel swelling. The calculational model used considers both the release to the grain boundaries of the gas and the swelling caused by the gas. The time for the gas to be released from the grain boundaries has not been calculated.

Some gas can be expected to escape from the grain boundaries during the relatively long time between clad failure and the start of fuel motion in a loss-of-flow experiment. The experimental data do not clearly indicate any significant gas release at the time the fuel melts. If released, the fission gas in the fuel probably directly influences fuel motion by sweeping out fuel particles or forcing the flow of molten fuel. The fission gas remaining in the fuel then causes fuel swelling, and the fission gas remaining on the grain boundaries causes the breakup of the fuel along the grain boundaries.

The conclusion is that the fission gas due to the preirradiation of fuel in experiments L3 and L4 was instrumental in keeping the fuel from collapsing as it did in experiment L2, but was not important as far as the fuel eructations are concerned.

V. RELATIONSHIP TO FTR

A. Fuel Pins

The fuel pins used in the fuel-dynamics loss-of-flow tests are similar to the FTR fuel pins in many respect but differ in several others. The cladding is the same: Type 316 stainless steel, 20% cold-worked, of prototypic diameter and thickness. The fuel is mixed oxide with a PuO enrichment slightly less than that in the FTR outer zone but greater than that in the FTR inner zone. The UO_2 is enriched in the test fuel while the UO_2 in the FTR pins is of natural enrichment. The smear density in the HEDL N-F pins is prototypic and in the PNL-17 pins is slightly greater than prototypic. All pellet dimensions are prototypic.

All the test pins had fuel-column lengths of 13.5 in. compared to the 36-in.-long FTR fuel columns. The test fuel-column length was the same as the height of the EBR-II core where the pins in L3 and L4 were irradiated. The overall fuel-pin length was also much shorter than the FTR fuel pins. The test pins were all designed with a shorter length for irradiation in EBR-II and were modified for use in the Mark-II loop.

Because of the relatively flat axial power profile in EBR-II, the irradiated test fuel pins had a microstructure which was essentially uniform over the length of the fuel column. By contrast, the larger FTR fuel pins will normally have a gradation in fuel microstructure from the ends toward to the middle. As indicated, the pins used in L3 had an "intermediate-power" microstructure with no central void, and the pins used in L4 had a "high-power" microstructure with a fully developed central void. Each test simulated the response of its microstructure to a loss-of-flow transient.

The short length of the fuel column means that both the average axial temperature gradient along the fuel and the total sodium temperature rise cannot be simultaneously duplicated. During the tests the pin axial power levels in the pins, and thus the axial temperature gradients, were within the range of those expected in FTR. The inlet sodium temperature at the start of each test was about 680°F, making the outlet temperature from each test prior to the reduction of flow approximately the FTR mixed

mean outlet temperature. Thus, as far as initial temperatures are concerned, the test temperatures to some extent simulated those to be expected in the top part of the fuel of a typical FTR fuel pin. The axial temperature profile in a test fuel pin and in a FTR-length fuel pin over the fuel length are shown in Fig. 26. The difference in axial temperature profile leads to a nonprototypical initial coolant-voiding phase in the tests.

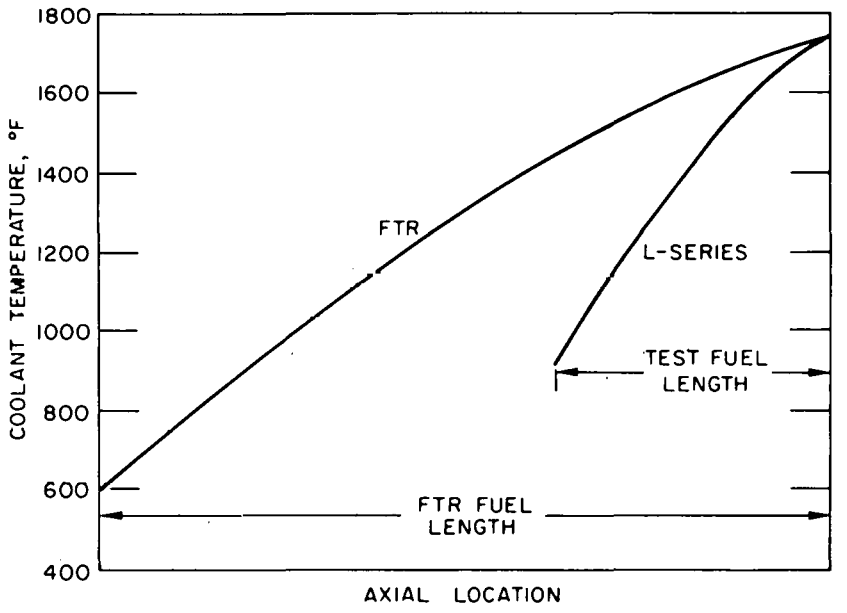

Fig. 26. Axial Coolant-temperature Profile.

The enriched uranium makes a difference in clad-fluence-to-fuel-burnup ratio for the irradiated test pins compared to FTR pins. Since the clad fails in a loss-of-flow test by melting, any mismatch of fluence to burnup is not important. In addition, changes in strength and ductility of annealed austenitic stainless steel are not substantial past a fluence of the order of 2×10^{22} nvt. The irradiations in EBR-II approached this fluence level for the pins used in L3 and L4.

The question of developing a prototypic fuel structure arises in testing both fresh and preirradiated fuels. In TREAT only a short operating time (a few seconds) can be achieved with the test fuel pins at the desired power level. During reactor-power changes, in particular during startup and shutdown, families of radial and circumferential cracks are produced in the fuel due to thermal stresses. These cracks will heal most rapidly in the inner hotter regions. In order to heat these cracks sufficiently such that the fuel structure is prototypic of long-term steady-state operation, operating times of a few weeks are required. Since fuel motion and the release of fission gas from the fuel in the preirradiated fuel tests appeared to be governed primarily by fuel melting, the lack of crack healing does not seem to be of major significance in influencing the sequence of events.

Variations in the axial fuel constraint of the test fuel pin and of pin-plenum sizes also do not appear to be significant with respect to initial fuel-element failure since failure occurred primarily from clad melting. Differences in postfailure behavior of the molten clad and fuel may in principle have been influenced by the differences in insulator pellets, reflector, and pin structure, as well as fuel-column length, and will be considered in discussing test-section characteristics.

B. Test-section Characteristics

The thermal-hydraulic and structural characteristics of the test section are important in comparing the test and reactor conditions. The cross section of the test section is shown in Fig. 3. The fuel pins in L2 and L3 had prototypic spacer wires whereas those in L4 were of a smaller diameter, 40 mils rather than the 54 mils used in FTR. This made for a tighter fuel bundle. In all the tests the fluted tube was designed to simulate the adjoining test pins within a cylindrical boundary. The adjoining spacer wires were not simulated, so the structural constraint on motion, particularly bending due to temperature gradients, was greater in the test bundle than would be expected in FTR.

Several cross-section parameters for the test section and for FTR are given in Table X. The first three quantities summarize general thermal-hydraulic properties of the test section compared to FTR. The most significant difference is the smaller ratio of heated perimeter to wetted perimeter for the test section. This implies that the surface for heat transfer per fuel pin to the fluted tube was greater than that to the subassembly wall in FTR. Note that the larger steel area in the tests than in FTR means that more heat could be absorbed in the fluted tube per fuel pin than in the FTR subassembly wall. The next two numbers compare clad and spacer-wire areas, and fuel areas to the flow area. The lower values of the ratios for the tests does not directly imply that the tests had more favorable conditions for fuel and clad motion. For example, the area available for molten-steel motion was larger, but the fluted tube provided a heat sink for the steel to freeze to. The last two ratios show how both the amount of molten steel and the available cross-section area available for the steel to move through increased once the fluted tube melted. Note that the ratios tend to compensate for one another as far as molten-steel motion is concerned. On the other hand, the molten fuel could move much more easily radially in the tests than in FTR once the fluted tube failed. This radial motion apparently occurred in the tests. The ratios given in Table X lead to qualitative statements about the similarity of the tests to what could be expected in FTR. The ratios also indicate the complexity involved in obtaining quantitative comparisons.

Several axial fuel-pin parameters and the corresponding ones for FTR are listed in Table XI. The differences in the lengths of the pins are of some importance with respect to fuel and cladding motion. The longer FTR fuel length can be expected to provide a larger amount of molten cladding and molten fuel per unit flow area than in the L-series tests. Thus the melting of FTR fuel pins might be expected to be more likely to cause flow blockage than the melting of the test fuel pins. Differences in the vapor velocities and the feasibility of sustained vapor flow in the tests as compared to FTR can also influence clad motion.

TABLE X. Cross-section Parameters of Test Section

Parameters	L2/L3	L4	FTR[a]
Flow area per pin (cm^2)	0.040	0.032	0.031 0.027
$\frac{\text{Heated parameter}}{\text{Wetted perimeter}}$[b]	0.539	0.565	0.748 0.805
Hydraulic diameter (in.)	0.120	0.100	0.128 0.119
$\frac{\text{Clad and spacer-wire area}}{\text{Flow area}}$	0.314	0.284	0.406 0.472
$\frac{\text{Fuel area}}{\text{Flow area}}$	0.783	0.985	1.02 1.18
$\frac{\text{Steel area}^c}{\text{Clad and spacer-wire area}}$	2.24	2.89	1.67 1.00
$\frac{\text{Total area}^d}{\text{Flow area}}$	2.4	3.1	-

[a]For the FTR the upper value is averaged over the subassembly and the lower value is for an isolated central fuel pin.

[b]Cladding perimeter, does not include spacer wire.

[c]Includes fluted tube, or subassembly can in FTR.

[d]Total area in flow area plus the area between the fluted tube and the outer wall of the adiabatic holder.

The axial fluted-tube temperatures in the L4 fuel pins during the loss-of-flow run are shown in Fig. 27. Note that although the temperatures above the top of the fuel column are nonprototypic (that is, the temperature drops rather than remains level at the start of boiling), at the time of fuel-pin failure the temperature distribution is prototypic. Thus when steel (or fuel) moves upward, it will move into a region with temperatures the same as those expected during a loss-of-flow accident in the FTR.

Note that in all three tests the cladding and fuel did not penetrate more than a few inches beyond the ends of the original fuel column. The difference in axial fuel penetration between L3, without an upper axial reflector, and L4, with a long upper insulator region, does not seem to be

TABLE XI. Axial Parameters of Test Section

Parameter	L2	L3	L4	FTR
Total pin length (in.)	20.875	30.875	42.984	95
Fuel length (in.)	13.5	13.5	13.5	36
Insulator pellets				
Top (in.)	0.5	0.5	6.7	0.5
Bottom (in.)	0.5	0.5	0.5	0.5
Axial reflector (Inconel)				
Top (in.)	6.0	0	5.0	5.7
Bottom (in.)	*	*	*	5.7
Plenum volume				
cm, in.	0.15	0.32	0.34	1.13

*A 3.4-in.-long solid steel, lower end fitting was below the insulator pellets in the test pins.

significant. When consideration is given to the prototypicality of temperature distributions above the fuel and the apparent lack of significant penetration, the tests seem to be quite relevant as far as the freezing out of molten material near the top of the fuel column is concerned.

The test inlet temperatures were, on the other hand, greater than those expected in FTR. Again the cladding and fuel did not penetrate very far downward, at least not past the lower steel end fitting. Thus freezing of molten materials during the tests near the bottom of the fuel is also quite similar to what would happen in FTR.

C. Loop Features

The Mark-IIA loop does not simulate a complete reactor subassembly with the inlet and outlet subassembly conditions matching those expected during a loss-of-flow transient. The loop instead provides a test bed for observing the meltdown of short fuel pins during a programmed reduction in pump power.

The Mark-IIA loop has a single flow path. The sequence of events in the test assembly (that is, coolant boiling, voiding, etc.) is dependent

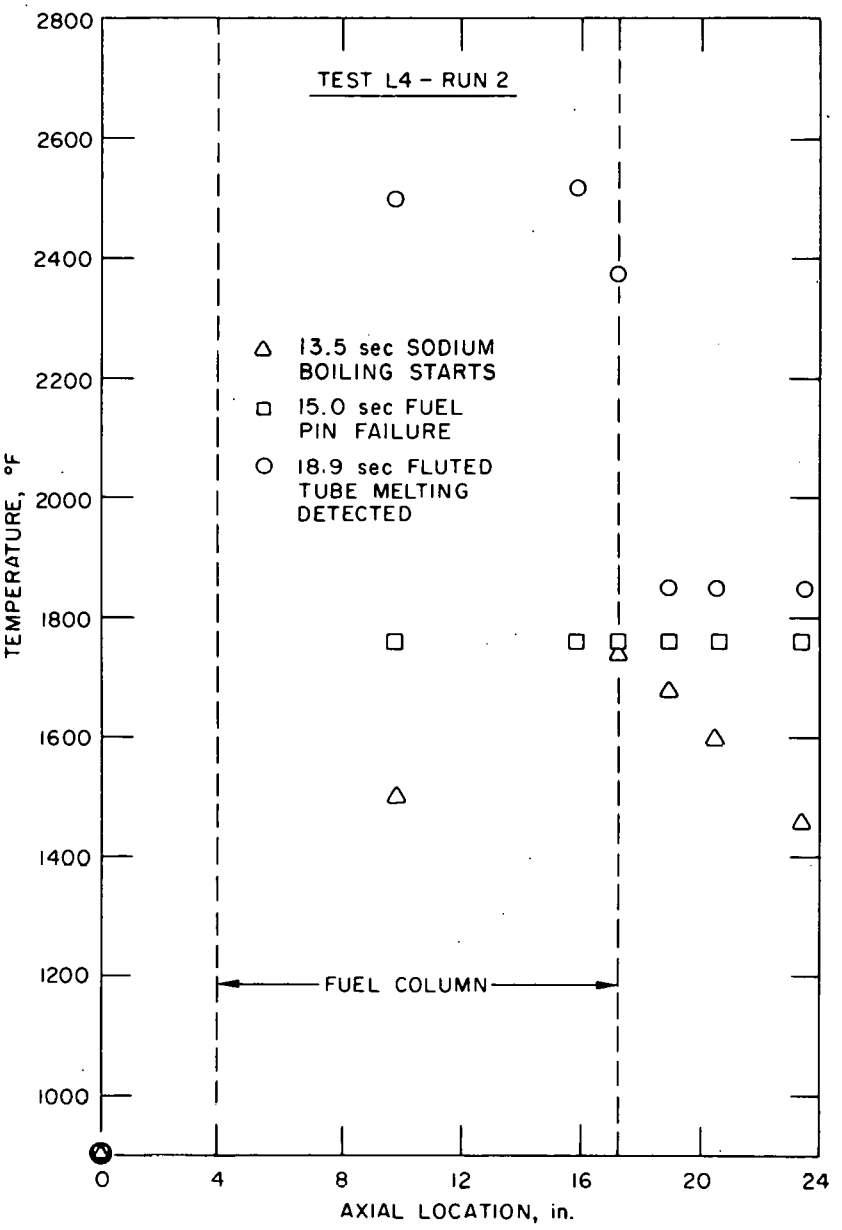

Fig. 27. Fluted-tube Temperatures for Test L4.

upon the thermal-hydraulic flow characteristics of the loop. The sequence of events during the loss of flow in a reactor would be expected to be less dependent upon the reactor-system characteristics and noncoherent from subassembly to subassembly, that is, some subassemblies would melt and the fuel move before the fuel pins in other subassemblies fail. In addition, the large mass of coolant in the plenums above and below the core and the larger cover-gas plenum in the reactor would make the inlet and outlet pressures during a reactor transient different from those in the loop. The loop has a short flow path, has a small loop plenum, and does not have a heat exchanger. Thus the inlet and exit pressures and temperatures of the test section are coupled through the pump side of the

loop. The coupling of the test-section inlet and outlet pressures is quite important, as this pressure differential is the driving force behind sodium-vapor streaming. Sodium-vapor streaming is thought to govern the motion of the molten steel, particularly of the cladding. Thus the loop differential would control the formation of cladding blockages and strongly influence the entire sequence of events. The release of fission gases during the test increased the ambient pressure in the loop. But the change in loop pressure and hence the sodium boiling temperature actually provides a means of detecting gas release during fuel-pin failure. As far as coolant inlet temperature is concerned, it reaches a maximum at the end of the flow reduction and then drops 10 to 20 degrees prior to failure of the inlet thermocouple. Note that the outlet thermocouples in test L4 actually measured the temperatures of the sodium in the upper part of the loop.

APPENDIX

SAS Analysis of Tests

A. Introduction

Calculations of the three Fuel Dynamics loss-of-flow tests L2, L3, and L4 have been done using the SAS2B code.[12] For each experiment both the heat balance and the flow-coastdown runs were analyzed, and the thermal histories of fuel, clad, and coolant calculated. Every effort was made to ensure that SAS input modeled as accurately as possible conditions and geometry of the tests considered.

The SAS2B code was developed at ANL to provide a flexible analytical tool which could be used in fast-reactor safety analyses. The code initializes thermal-hydraulic conditions defining the preaccident steady operating state of the system via a steady-state initialization routine. Transient history of the system from a specified power increase or specified reduction of coolant flow is then calculated. Coolant boiling and voiding, clad melting and relocation, and fuel melting and slumping can be followed. The code therefore furnishes a tool with which to analyze loss-of-flow tests.

The physical situation represented by the code is a single "average" pin of the seven-pin cluster with associated coolant and structure. Figure A-1 depicts the model. Due to the single-pin limitation, SAS2B cannot directly account for all the multidimensional features inherent in the tests; however, it is capable of analyzing the behavior of fuel, clad, and coolant after coolant boiling has started. Table A-1 lists the geometric parameters used in the calculations. Since SAS assumes a constant cross section for sodium flow, the inertial lengths and reflector lengths were adjusted to account for the differences in friction due to differences in flow area.

B. Calculations for Heat-balance Run

Each of the three flow-coastdown experiments was preceeded by a heat-balance run in which the power transient was duplicated without flow rundown. The heat-balance runs are tests L2-1, L3-1, and L4-1. As the name implies, this preparatory transient was used to establish a heat balance on the pin bundle and verify the calibration factor. In each run a value of 4.9 W/g-MW was found to give satisfactory predictions of measured temperatures. The probable accuracy of the calibration factor is ±0.2 W/g-MW or ±4%. As identical TREAT core loadings and similar control-rod motions were used during the coastdown transient as during the heat-balance runs, the calibration factor is taken to be the same in both cases.

Experimental data and the SAS calculation values for test L2-1 are shown in Figs. A-2, A-3, A-4, and A-5. The agreement between the calculated and experimented values is very good.

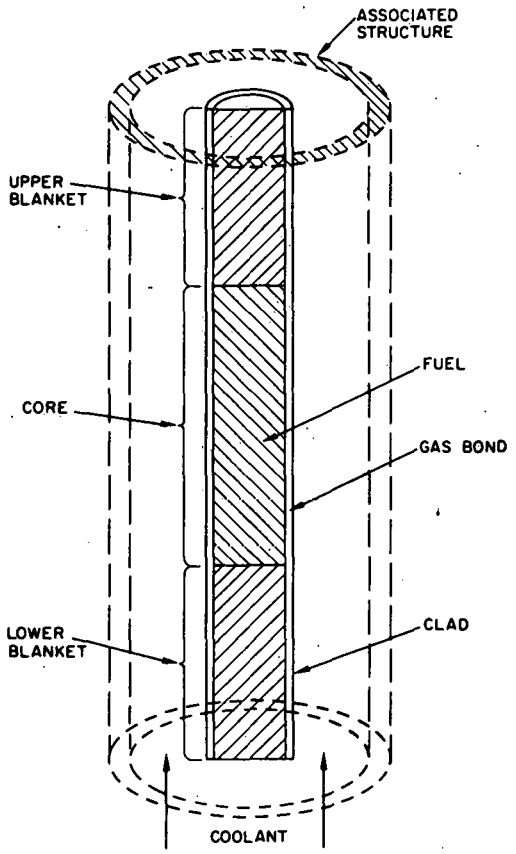

Fig. A-1.
Single Fuel Pin, Coolant Channel, and Structure.

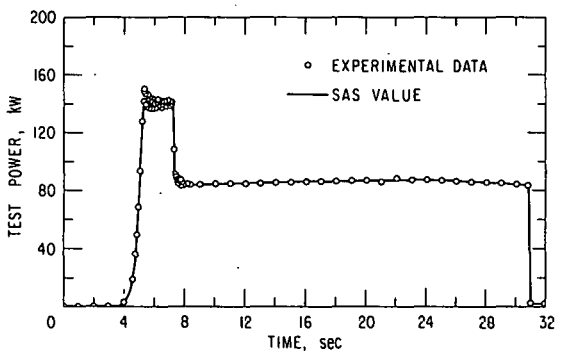

Fig. A-2.
L2-1 Test Power.

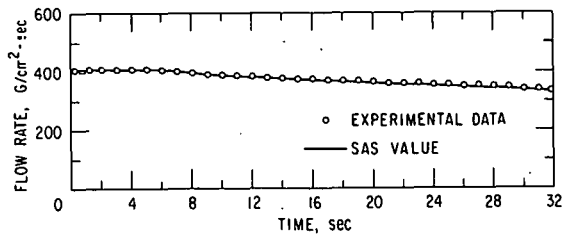

Fig. A-3.
L2-1 Inlet Flow.

TABLE A-1. SAS Geometrical Input Parameters

SAS Model	Input Length (cm)	Input No. of Nodes	Portion of Experiment Represented
Inertial length above core	5	-	Sodium above pump return
Upper reflector	16	2	Loop from fluted-tube outlet to pump return
Gas plenum	20 (40)*	5	Gas plenum above tube and upper end cap
Upper blanket	15	4	Gas plenum with reflector
	1.27	1	Upper insulator pellets
Core	34.3	12	Fuel
	1.27	1	Lower insulator pellets
Lower blanket	8.6	2	Lower end cap
Lower reflector	80	3	Pump and pipe from pump to test section
Inertial length below core	40	-	Sodium above pump

*L4 value.

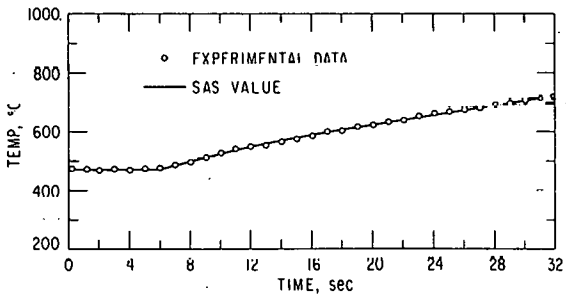

Fig. A-4.
L2-1 Inlet Sodium Temperature.

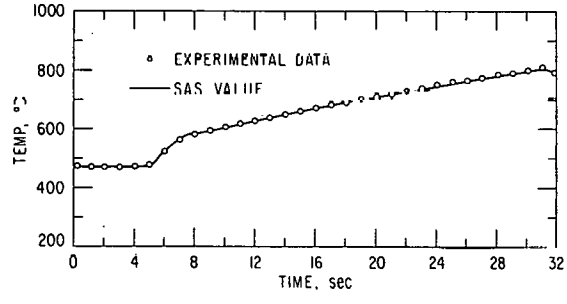

Fig. A-5.
L2-1 Outlet Sodium Temperature.

Similar plots for test L3-1 are shown in Figs. A-6, A-7, and A-8. Again, good agreement between measured and predicted outlet temperatures is obtained. Although not shown, generally good agreement was also obtained between measured and predicted fluted-tube temperatures.

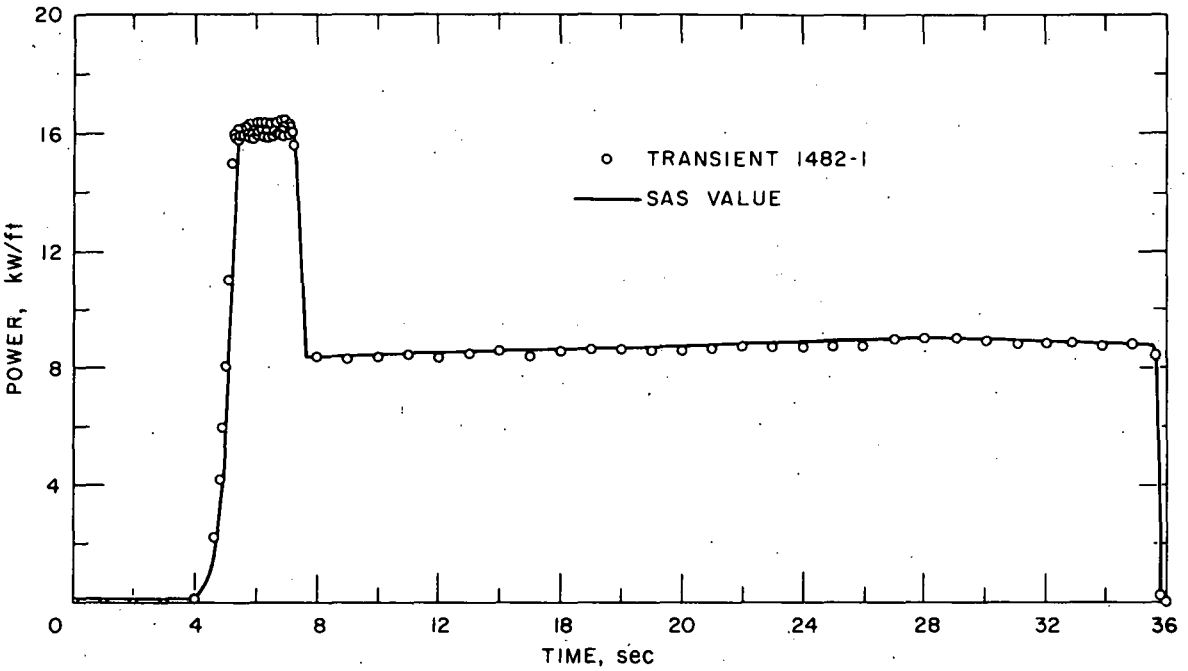

Fig. A-6. L3-1 Test Power.

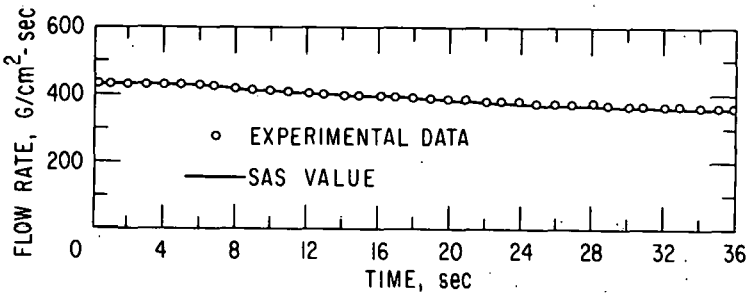

Fig. A-7. L3-1 Inlet Flow.

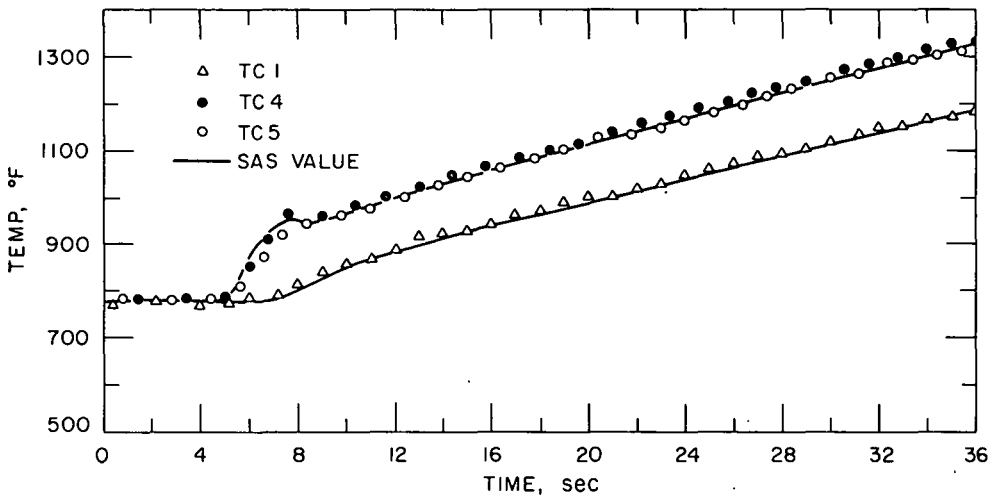

Fig. A-8. L3-1 Inlet and Outlet Sodium Temperatures.

Plots for test L4-1 are shown in Figs. A-9, A-10, A-11, and A-12. In this case, because of difficulties with sampling the analog tape

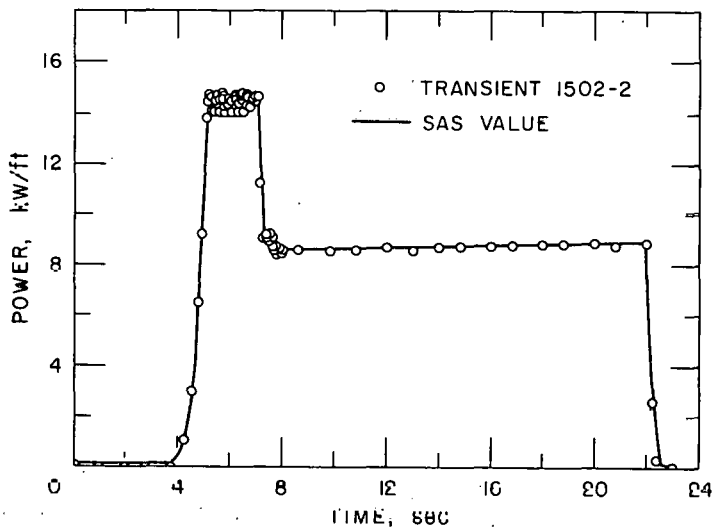

Fig. A-9. L4-1 Test Power.

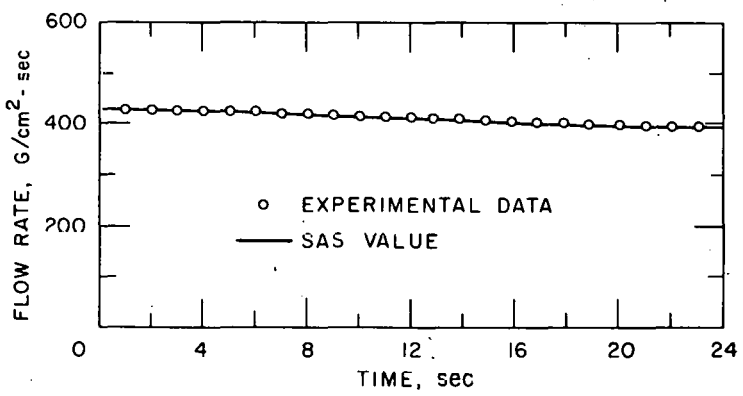

Fig. A-10. L4-1 Inlet Flow.

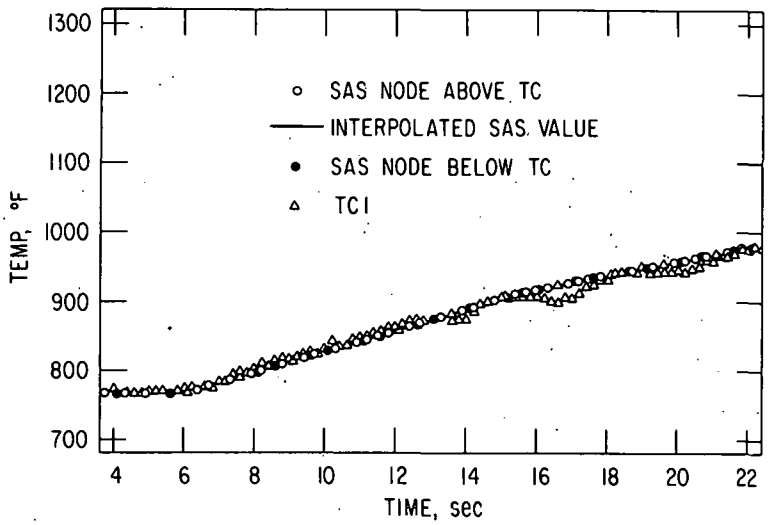

Fig. A-11. L4-1 Inlet Sodium Temperature.

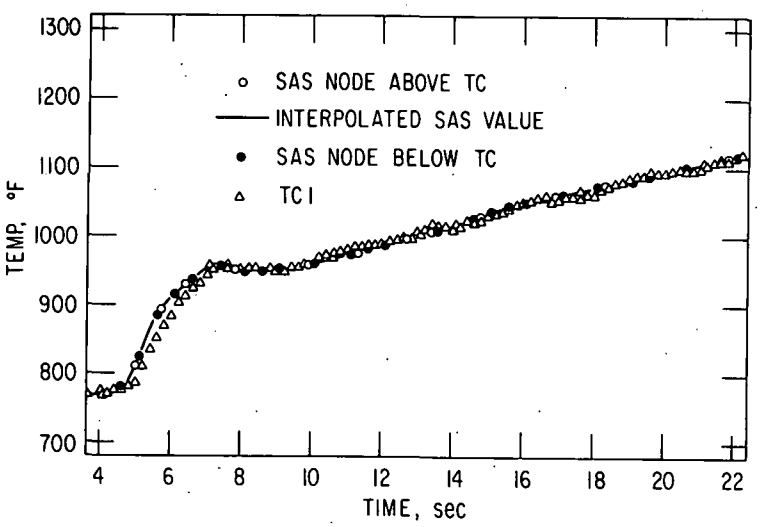

Fig. A-12. L4-1 Outlet Sodium Temperature.

recording, the inlet flow data in Fig. A-10 were taken from the oscillograph record of the test. Comparison of calculated and measured sodium outlet temperature was not practical because of the longer length of the fuel pins used in the L4 experiment. The longer length of the fuel pin led to heat losses from the sodium after leaving the adiabatic holder, which are not modeled in SAS. Thus, the heat balance is based on comparison of calculated and measured fluted-tube temperatures at TC11, as shown in Fig. A-12.

In summary the generally good prediction of bulk coolant and structure temperatures by the one-dimensional average-pin SAS model suggests a high degree of coolant flow mixing in the heat-balance runs.

C. Flow-coastdown Calculations

The SAS model used for heat-balance calculations was also applied to calculate the flow-coastdown transients (Runs L2-3, L3-2, and L4-2). Selected results for each of the three tests are discussed. Input values include the power transient, the inlet temperature, and a pump pressure versus time curve tailored to produce the measured inlet flow during the transient. Comparisons are made for inlet and outlet flow rates; clad and fuel temperatures are calculated; and structure temperatures are calculated for comparison with measured temperatures.

Plots pertaining to test L2-3 are given in Figs. A-13 through A-17. The calculated amplitude of inlet flow oscillations can be seen to greatly

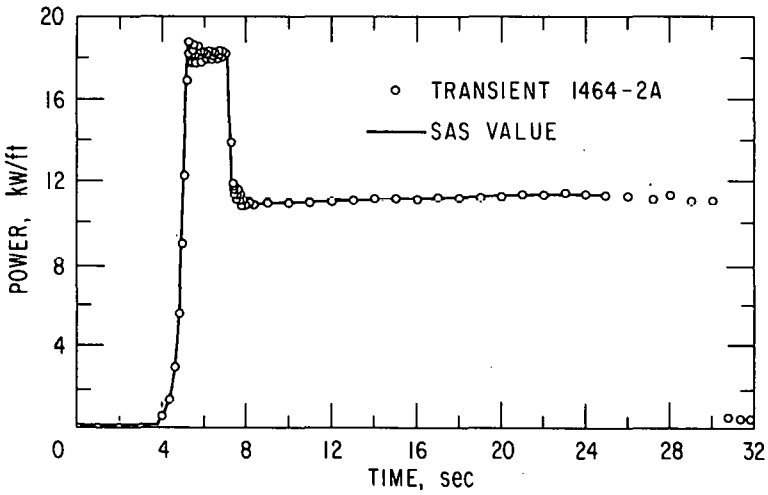

Fig. A-13.
L2-3 Test Power.

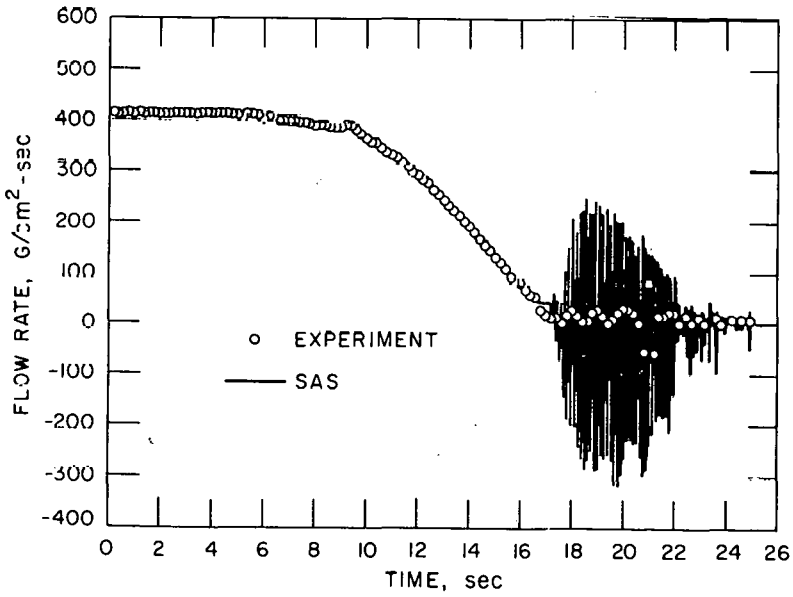

Fig. A-14.
L2-3 Outlet Flow.

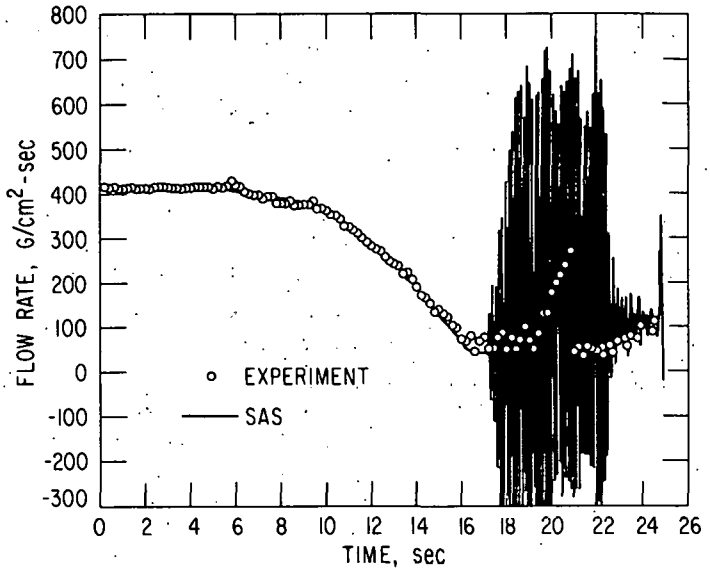

Fig. A-15.
L2-3 Outlet Flow.

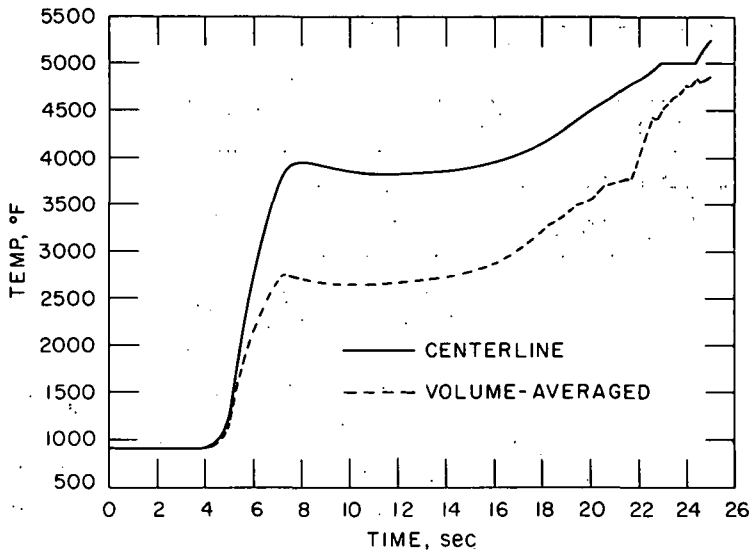

Fig. A-16.
L2-3 Fuel Temperature at Axial Midplane.

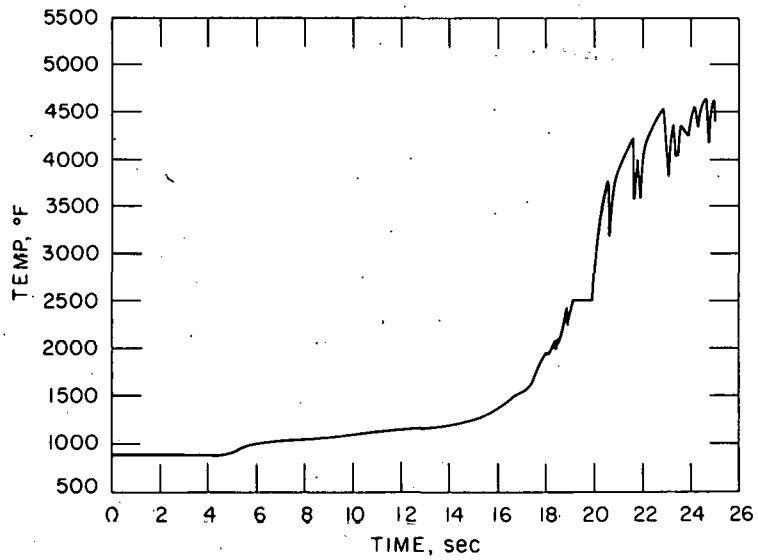

Fig. A-17.
L2-3 Clad Temperature at Axial Midplane.

exceed the measured value. Flow reversal is indicated essentially immediately at the inception of boiling. Likewise, very large oscillations are predicted in the outlet flow. These overpredictions are probably due to the one-dimensional nature of the boiling model in SAS, which does not represent very well the two-dimensional voiding in the test, that is, voiding in the test likely started in the central subchannels while the peripheral subchannels still contained liquid sodium. The flow pattern would then be annular with a significant liquid sodium film near the cold wall. However, the SAS model assumes that vapor fills the cross section except for thin liquid films on the surfaces. Thus, a downward growth of the voided region necessarily results in inlet flow reversal.

The calculated fuel and clad temperatures at the axial midplane of the fuel are given in Figs. A-16 and A-17. Note that nearly steady-state temperatures are indicated during the duration of the flow coastdown, followed by a rapid rise (∿450°F/sec) in clad temperature after boiling and dryout. The rise in fuel temperature is somewhat slower.

Figure A-18 is a diagram comparing various events observed in the test with predictions based on SAS calculations. The inception of boiling

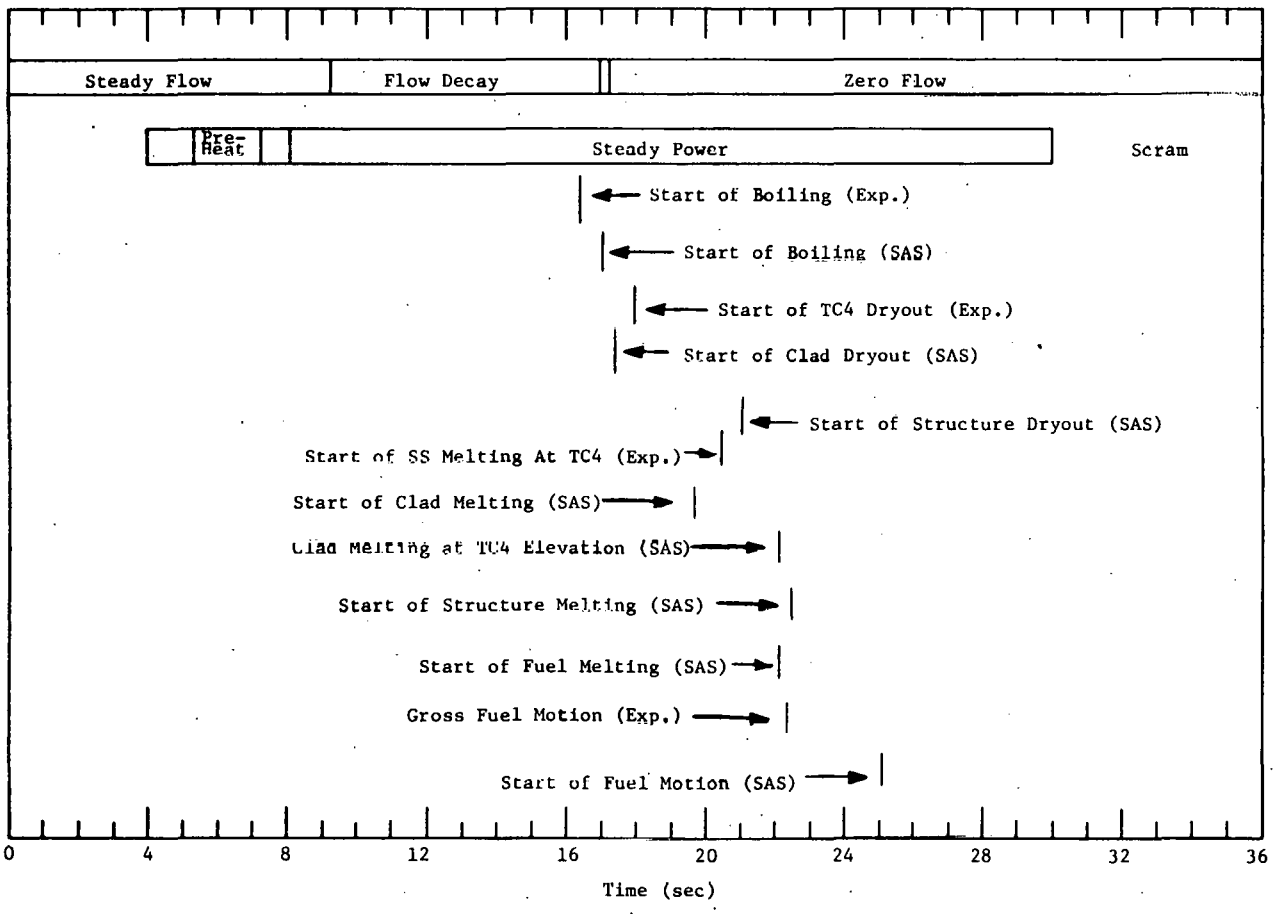

Fig. A-18. Comparison of Experiment with SAS Predictions for L2-3.

is predicted reasonably well, but subsequent events are predicted to occur somewhat later than was experimentally observed. Generally the proper sequence of events is predicted, but the timing is not very accurate. Of course, such events as dryout and clad melting are not directly observed, so that an exact comparison cannot be made. Also, the one-dimensional treatment of voiding will influence the predictions of clad motion.

Slumping as indicated in Fig. A-18 is based on 95% of the fuel area reaching the solidus or above at the hottest axial node. The predicted time of inception of slumping is about 3 sec later than the observed time. The criterion for slumping in the SAS code is probably not realistic, since the most likely mechanism for the observed slumping is the collapse of the fuel-pellet column after the clad melts. If the criterion for collapse of the fuel-pellet column is taken to be the inception of clad melting over the full height of the fuel column, the collapse would be predicted to occur within less than a second of the observed collapse.

The abrupt dispersal or eructation of fuel observed late in the transient is not predicted by SAS since the code used does not contain a model for that particular phenomenon. The eructations could be predicted using a mechanism of stainless steel and fuel vapor pressures acting on molten fuel. Such a model is under development.

Calculated values and experimental data for test L3-2 are shown in Figs. A-19 through A-24. The results are similar to those obtained for

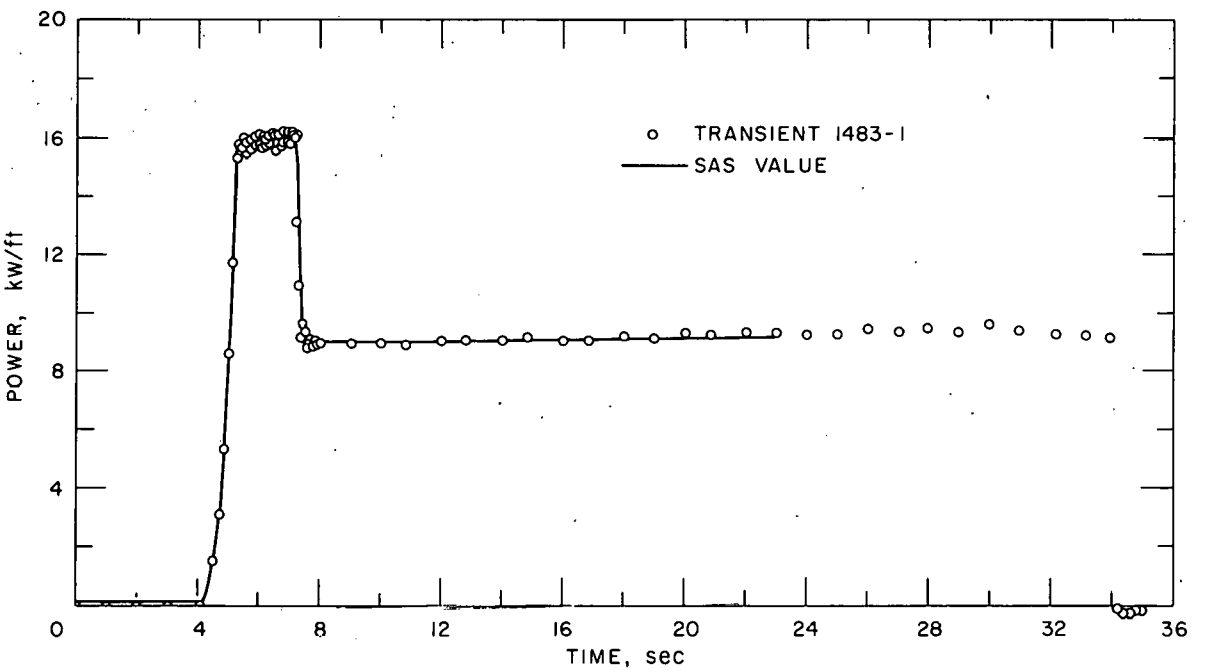

Fig. A-19. L3-2 Test Power.

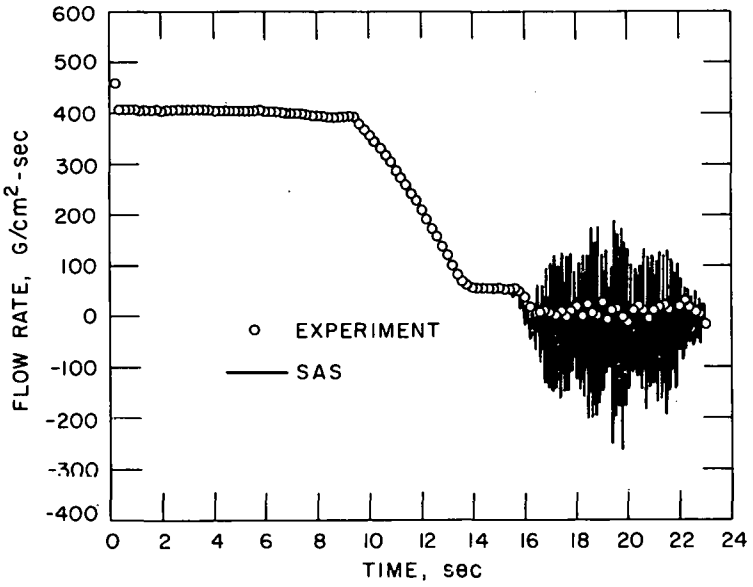

Fig. A-20.
L3-2 Inlet Flow.

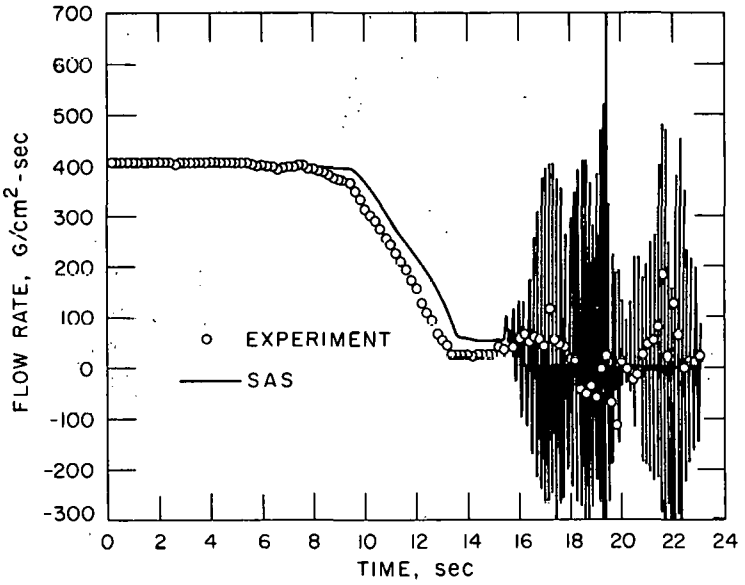

Fig. A-21.
L3-2 Outlet Flow.

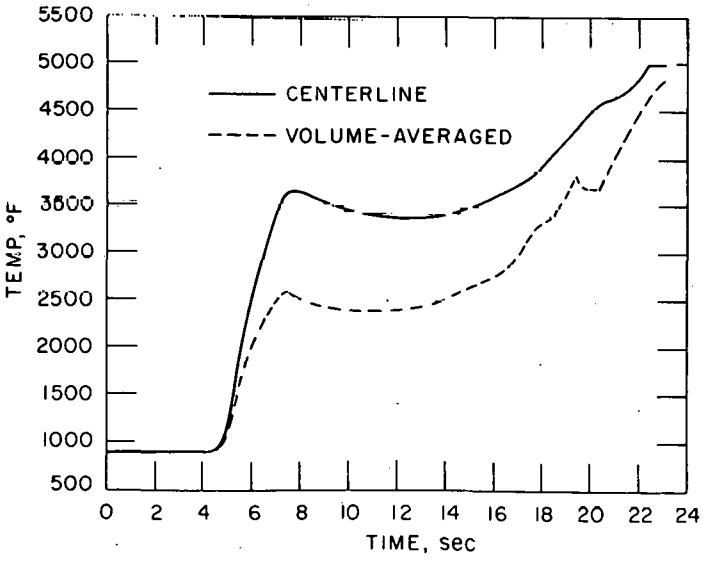

Fig. A-22.
Fuel Temperature at Axial Midplane.

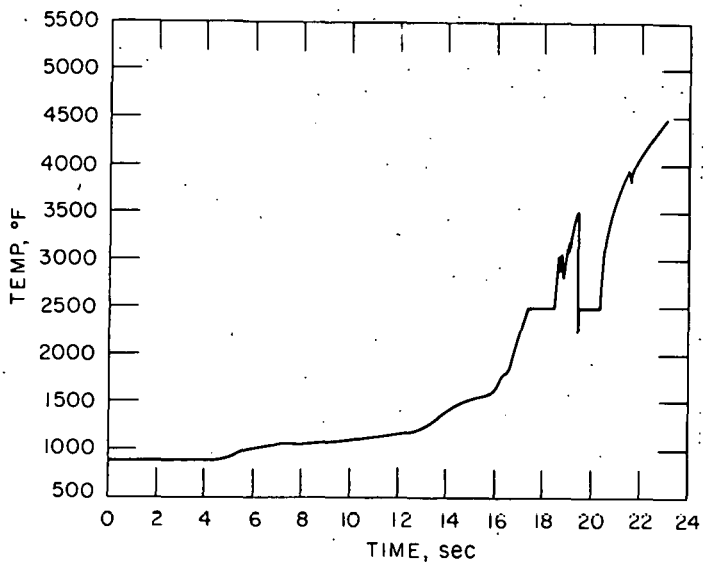

Fig. A-23.
L3-2 Clad Temperature at Axial Midplane.

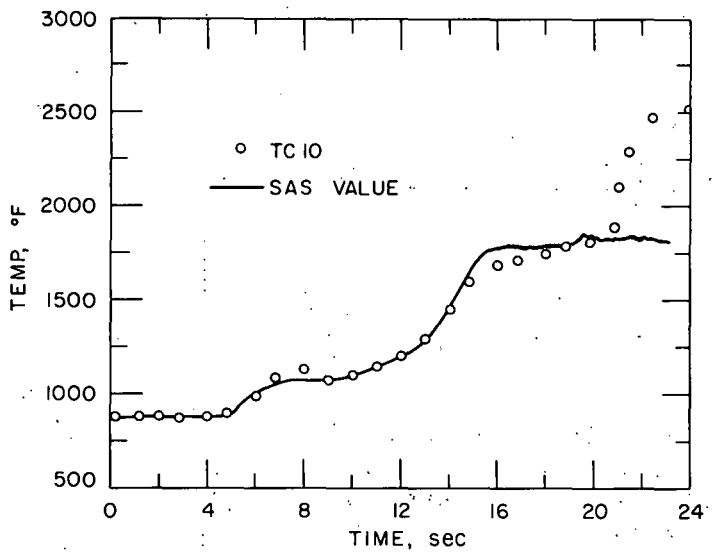

Fig. A-24.
L3-2 Structure Temperature at Top of Fuel Column.

test L2-3 in that high-amplitude flow oscillations are predicted but were not observed. The difference between measured and calculated outlet flow during the coastdown (see Fig. A-21) is caused by a distortion in the outlet-flowmeter signal. Reasonably good agreement between the calculated and measured structure temperature at the top of the fuel column occurs until late in the transient. The observed temperature excursion to melting is not predicted, but good agreement is obtained between predicted structure dryout and the beginning of the temperature excursion.

Figure A-25 presents a comparison scenario for test L3-2. Again, as in L2-3, agreement on the time of boiling inception is good. SAS predicts clad melting prior to the time at which the fission gases appear to be released to the plenum, as indicated by an experimental pressure rise. Since gas release should occur at or before clad melting, the prediction is too early. Good agreement occurs for the time of structure dryout.

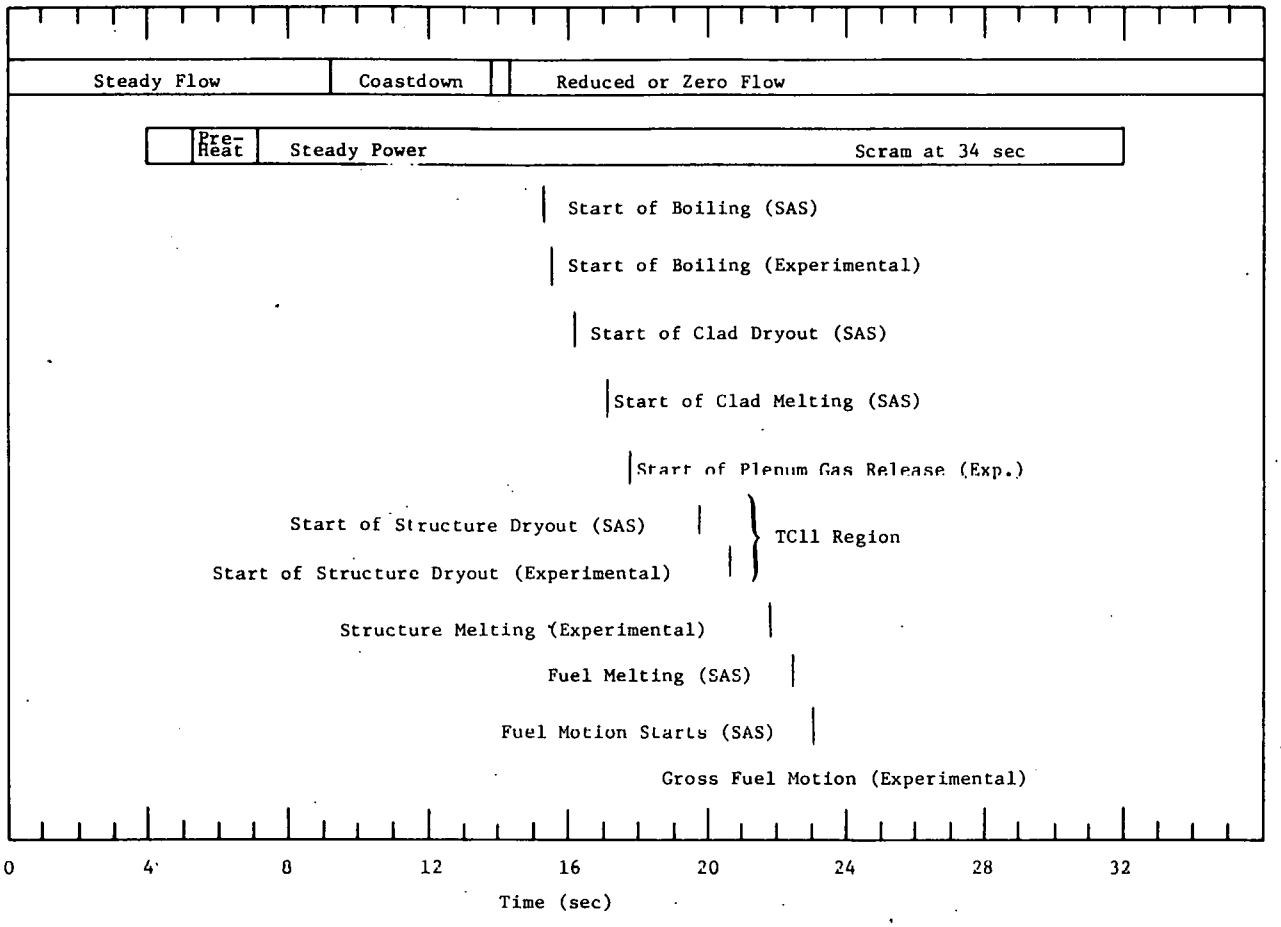

Fig. A-25. Comparison of Experiment with SAS Predictions for L3-2.

Fuel motion is predicted at about 23 sec based on the slumping criterion of 50% of the radial node forming the boundary between the equiaxed and unrestructured fuel region reaching liquidus. Some motion is observed around this time, but it is not of the fuel-slumping type predicted by the model. No gross motion is observed until an eructation late in the transient.

Plots for test L4-2 are illustrated in Figs. A-26 through A-31. Note that while the flow oscillations are still overpredicted, the amplitude is less than in previous calculations. Again, a distortion of the outlet flow signal is evident. The comparison scenario (see Fig. A-32) indicates reasonable agreement between SAS predictions and observations. Observed slumping of the fuel in the central pin begins at about 21.7 sec. Predicted slumping begins at 20.4 sec. The agreement in time is better than that obtained for previous tests.

The SAS calculations provide a certain amount of qualitative guidance in the interpretation of test results. As an example, during the period of time that SAS calculations indicate clad melting, only a gradual rise in structure temperature occurs. Consequently caution must be exercised when

using data from the fluted-tube thermocouples to infer clad conditions. In general, SAS appears to furnish a reasonable and valuable scenario of events for the loss-of-flow tests.

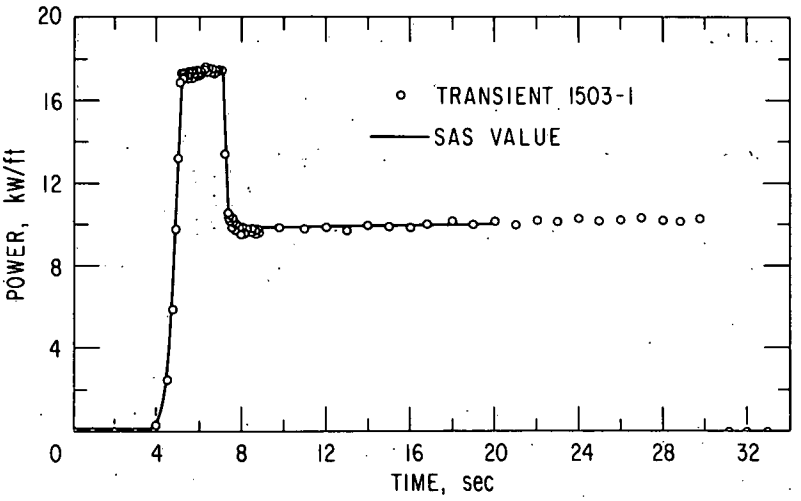

Fig. A-26. L4-2 Test Power.

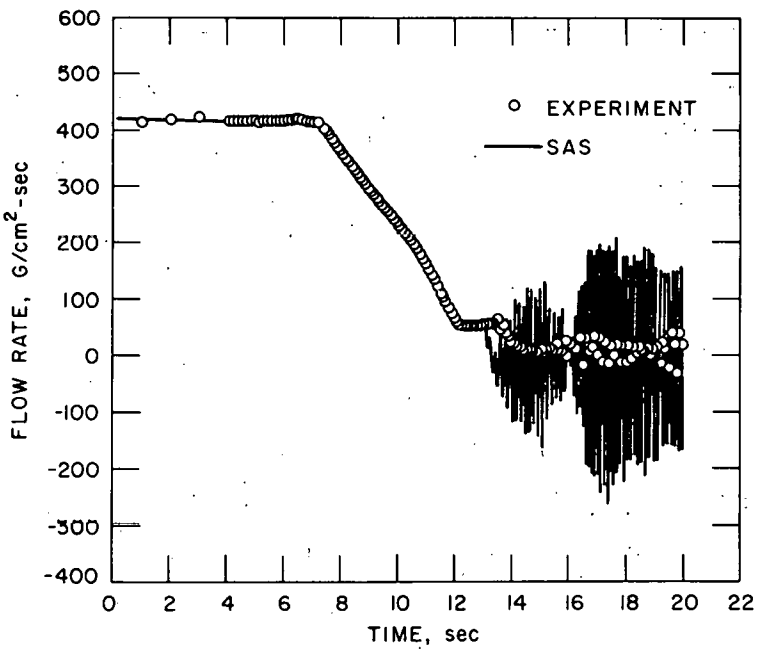

Fig. A-27. L4-2 Inlet Flow.

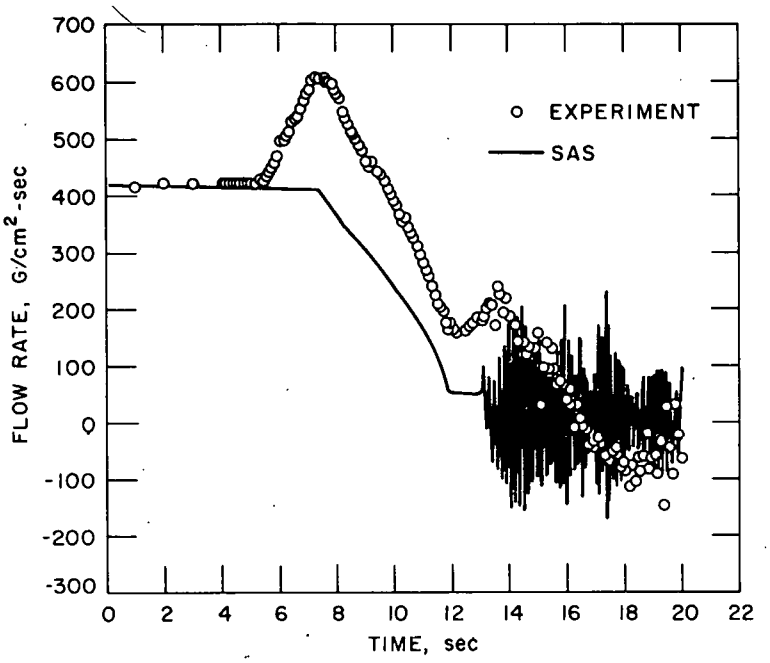

Fig. A-28. L4-2 Outlet Flow.

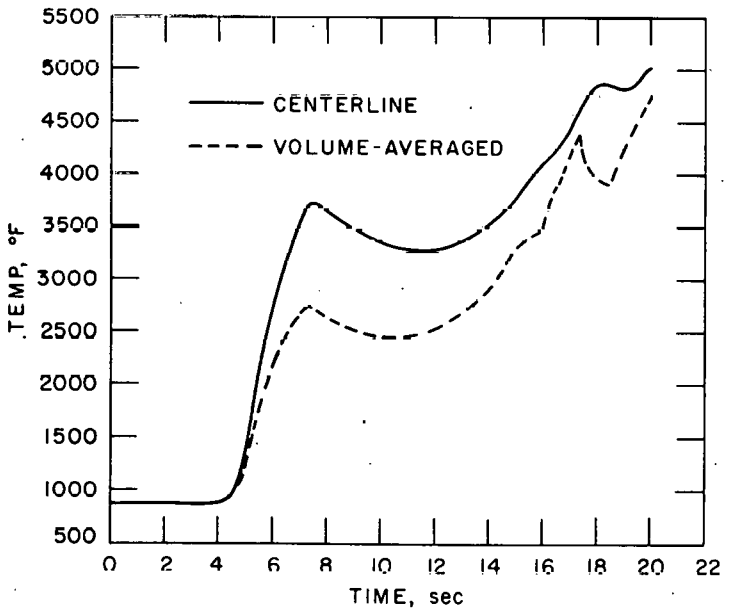

Fig. A-29. L4-2 Fuel Temperature at Axial Midplane.

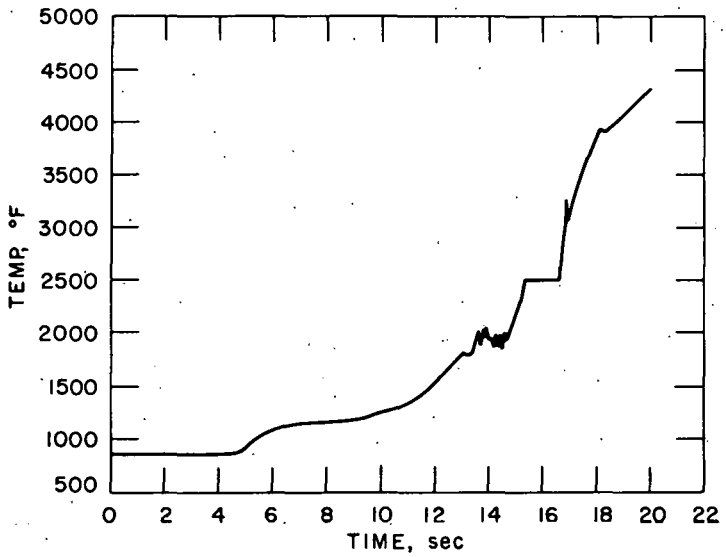

Fig. A-30. L4-2 Clad Temperature at Axial Midplane.

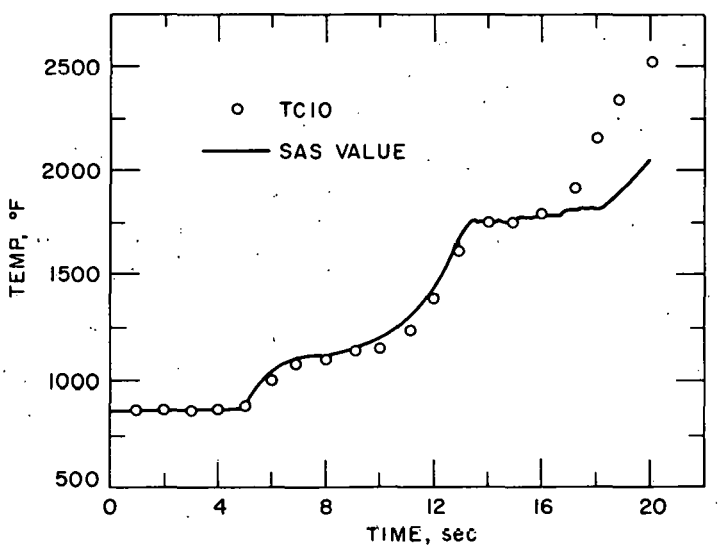

Fig. A-31. L4-2 Structure Temperature at Top of Fuel Column.

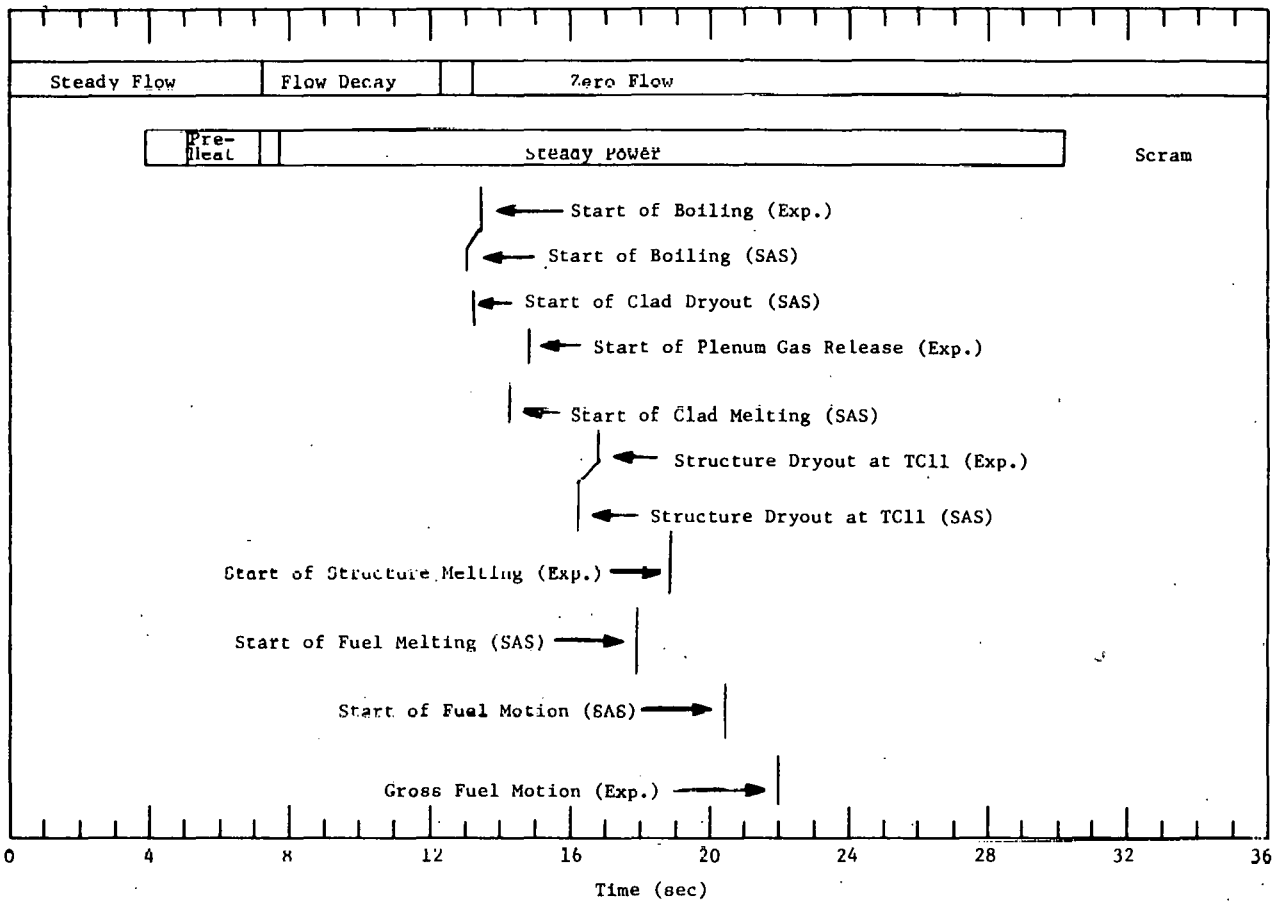

Fig. A-32. L4-2 Comparison of Experiment with SAS Predictions for L4-2.

ACKNOWLEDGMENTS

The authors wish to acknowledge the contributions of the many persons and groups involved in the preparation, conduct, and analysis of the tests.

Overall management of the program was the responsibility of C. E. Dickerman and R. O. Ivins. Technical leadership of the program from its inception was provided by C. E. Dickerman. Planning and preparation for test L2 was under the direction of J. C. Carter. In addition, L. W. Deitrich, B. A. Feay, and J. G. Eberhart participated in performance of the experiment and analysis of the results. The lead experimenter for tests L3 and L4 was L. W. Deitrich. E. W. Barts, A. K. Fischer, J. G. Eberhart, and C. C. Meek conducted posttest evaluations. J. P. Tylka assisted in the performance of tests L3 and L4. Fuel-characterization data was assembled by R. G. Palm.

Development of the Mark-II loop system was originated by L. E. Robinson; loop outfitting was conducted by K. J. Schmidt, R. T. Purviance, R. J. Schlitz, E. R. Maslowicz, J. E. Emerson, J. P. Burghardt, C. August, and G. G. Dewey. More recently, leadership in test engineering and operations has been provided by R. A. Noland, with able assistance from H. V. Rhude, J. P. Burelbach, and V. M. Kolba. Significant contributions in data management, computer graphics, and computer-codes development and usage have been made by P. H. Froehle. Assistance in performance of the SAS calculations was provided by W. R. Bohl and T. J. Heames. Handling of loops and test sections in Idaho has been directed by J. H. Cook, D. L. Mitchell, and J. F. Kerr at HFEF. TREAT operations, including data acquisition, has been under the direction of J. F. Boland and L. J. Harrison. Pre- and posttest metallurgical examinations have been conducted under the leadership of L. A. Neimark, W. F. Murphy, and D. Stahl. Hodoscope operation and data interpretations have been directed by A. DeVolpi, with assistance from G. S. Stanford, R. R. Stewart, and J. P. Regis.

REFERENCES

1. L. W. Deitrich et al., *A Loss-of-flow Simulation with Fresh FFTF-type Fuel Pins*, Trans. Am. Nucl. Soc., *16*, 182 (1973); A. DeVolpi et al., *Fast-Neutron Hodoscope Visualization of Fuel Movement in a Seven-pin Loss-of-flow Simulation*, Trans. Am. Nucl. Soc., *16*, 182 (1973).

2. E. W. Barts et al., *Loss-of-flow Simulation with Preirradiated FFTF-type Fuel Pins (Tests L3 and L4)*, Trans. Am. Nucl. Soc., *17*, 363 (1973).

3. L. W. Deitrich et al., *Fuel Dynamics Experiments Supporting FTR Loss-of-flow Analysis*, Proc. of Fast Reactor Safety Topical Meeting of the American Nuclear Society, Beverly Hills, California, April 2-4, 1974, p. 239.

4. W. R. Bohl and M. G. Stevenson, *A Fuel Motion Model for LMFBR Unprotected Loss-of-Flow Accident Analysis*, Presented at the National Topical Meeting on Mathematical Models and Computational Techniques for Analysis of Nuclear Systems, April 9-11, 1973, Ann Arbor, Michigan.

5. A. B. Rothman et al., Trans. Am. Nucl. Soc., *13*(2), 652 (1970).

6. G. A. Freund, P. Elias, D. R. MacFarlane, J. D. Geier, and J. F. Boland, *Design Summary Report on the Transient Reactor Test Facility (TREAT)*, ANL-6034 (1960).

7. L. E. Robinson, R. T. Purviance, and K. J. Schmidt, *The Mark-II Integral Sodium TREAT Loop*, ANL-7692 (1971).

8. A. DeVolpi, R. R. Stewart, and L. W. Deitrich, *Fast-Neutron Hodoscope Visualization of Fuel Movement in a Seven-pin Loss-of-flow Simulation*, Trans. Am. Nucl. Soc., *16*, 182 (1973); E. T. Weber, O. D. Slagle, and C. A. Hinman, *Laboratory Studies on Melting and Gas Release Behavior of Irradiated Fuel*, HEDL-SA-699, Presented at the American Nuclear Society Fast Reactor Safety Meeting, April 2-4, 1974, Los Angeles, California.

9. R. L. Fish et al., *Strain Response and Failure of 20% Coldworked 316 Stainless Steel Cladding During Temperature Transients*, HEDL Monthly Technical Progress Report (May 1973), (HEDL-TME 73-4, Vol. 1).

10. R. R. Stewart, C. E. Dickerman, L. E. Robinson, and W. B. Doe, *Studies of Fast Reactor Fuel Element Behavior under Transient Heating to Failure*, ANL-7552 (1969).

11. M. G. Chasanov, L. Leibowitz, and S. D. Gabelnick, *High Temperature Physical Properties of Fast Reactor Materials*, J. Nucl. Materials, *49*, 129-135 (1973/74).

12. W. R. Bohl and T. J. Heames, *A Clad Motion Model for LMFBR Loss-of-Flow Accident Analysis*, Trans. Am. Nucl. Soc., *17*, 358 (1973).